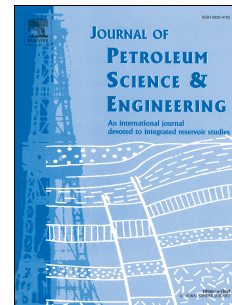


# Journal Pre-proof

Tight tuff reservoir characteristics and its controlling factors: A comparative study of the Permian Tiaohu Formation and Carboniferous Haerjiawu Formation in the Santanghu Basin, NW China

Jian Ma, Guoheng Liu, Zhilong Huang, Guangxi Ou, Tianjun Li, Xiaobo Guo



PII: S0920-4105(19)31227-6

DOI: <https://doi.org/10.1016/j.petrol.2019.106808>

Reference: PETROL 106808

To appear in: *Journal of Petroleum Science and Engineering*

Received Date: 24 February 2019

Revised Date: 2 December 2019

Accepted Date: 13 December 2019

Please cite this article as: Ma, J., Liu, G., Huang, Z., Ou, G., Li, T., Guo, X., Tight tuff reservoir characteristics and its controlling factors: A comparative study of the Permian Tiaohu Formation and Carboniferous Haerjiawu Formation in the Santanghu Basin, NW China, *Journal of Petroleum Science and Engineering* (2020), doi: <https://doi.org/10.1016/j.petrol.2019.106808>.

This is a PDF file of an article that has undergone enhancements after acceptance, such as the addition of a cover page and metadata, and formatting for readability, but it is not yet the definitive version of record. This version will undergo additional copyediting, typesetting and review before it is published in its final form, but we are providing this version to give early visibility of the article. Please note that, during the production process, errors may be discovered which could affect the content, and all legal disclaimers that apply to the journal pertain.

© 2019 Published by Elsevier B.V.

# **Tight tuff reservoir characteristics and its controlling factors: a comparative study of the Permian Tiaohu Formation and Carboniferous Haerjiawu Formation in the Santanghu Basin, NW China**

Jian Ma<sup>a, c\*</sup>, Guoheng Liu<sup>b\*</sup>, Zhilong Huang<sup>c</sup>, Guangxi Ou<sup>a</sup>, Tianjun Li<sup>c</sup>, Xiaobo Guo<sup>d, e</sup>

<sup>5</sup> <sup>a</sup>Beijing Research Institute of Uranium Geology, Beijing 100029, China

6 <sup>b</sup> Oil and Gas Survey, China Geological Survey, Beijing, 100083, China

<sup>7</sup> <sup>c</sup> State Key Laboratory of Petroleum Resource and Prospecting, China University of Petroleum, Beijing  
<sup>8</sup> 102249, China

<sup>9</sup> <sup>d</sup> School of Earth Sciences and Engineering, Xi'an Shiyou University, Xi'an 710065, China

<sup>10</sup> *eShaanxi Key Laboratory of Petroleum Accumulation Geology, Xi'an Shiyou University, Xi'an 710065,*  
<sup>11</sup> *China*

12     **Abstract:** Tight oil resources have been found in tight tuff reservoirs in many oil and gas bearing basins.

13     The tight tuff reservoir developed in the Santanghu Basin (NW China) has provided an excellent

14     opportunity for further research to enhance our cognition and understanding of tuff reservoir characteristics.

15     This study focuses on the differences in the basic characteristics in petrologic features, reservoir space, and

16     physical properties between the Tiaohu and Haerjiawu formations tuff reservoirs, then determines the

17     formation mechanism causing these differences. (1) The tuff samples of the Tiaohu Formation mainly

18     consist of vitric fragments, and quartz and albite are the major mineralogical components. However, the

19     crystal fragment content is much higher in the Haerjiawu Formation tuff, and albite and anorthite are the

20     major components. (2) Primary pores and the interparticle pores among authigenic minerals formed during

21     alteration are the main pore types for both the Tiaohu Formation and Haerjiawu Formation tuffS. (3) The

22     Tiaohu Formation tuff reservoir is characterized by high porosity (ranging from 10% to 25%) and

23 relatively low permeability (on the order of 0.01–0.50 mD), while that of the Haerjiawu Formation is  
 24 characterized by lower porosity (<10%) and lower permeability (mainly <0.1 mD). (4) Alteration and  
 25 compaction processes contributed most to the pore formation in both the Tiaohu and Haerjiawu tuff  
 26 reservoirs. Hence, the changes in total tuff reservoir porosity can be explained by the evaluation of  
 27 compaction residual porosity and alteration porosity. The vitric fragments in the Tiaohu Formation  
 28 originated from acidic or intermediate-acidic volcanic ashes, which are more liable to be altered than the  
 29 basic volcanic ashes that formed the crystal fragments in the Haerjiawu Formation. Moreover, the  
 30 Haerjiawu Formation tuff reservoir is buried hundreds of metres deeper than the Tiaohu Formation in  
 31 general, and thus, experienced stronger diagenetic compaction, which indicates fewer residual pores for  
 32 Haerjiawu Formation tuff samples. The nature of tuff and the deeper burial depth are the major reasons for  
 33 the worse physical properties of the Haerjiawu Formation tuff reservoir.

34 **Keywords:** tight tuff reservoir; porosity; alteration; Haerjiawu Formation; Santanghu Basin

## 35 1. Introduction

36 Tight oil generally refers to the accumulation of petroleum in tight sandstones, tight carbonates and  
 37 shale, and increasingly contributes to the energy supply (Cui et al., 2019; Ma et al., 2019; Tian et al., 2019).  
 38 Following the recent rapid increase in shale gas production, petroleum in tight reservoirs has become  
 39 another new field for unconventional hydrocarbon exploration and development worldwide (Kuhn et al.,  
 40 2012; Wang et al., 2014; Cao et al., 2016; Zhao et al., 2018). Tight reservoirs, such as tight sand and shale,  
 41 usually requires multi staged hydraulic fracturing in horizontal wells for commercial production because of  
 42 low porosity and permeability (Flewelling et al., 2013; Liu et al., 2016, 2018; Zhao et al., 2018). Apart  
 43 from tight sand and shale reservoirs, oil and gas has already been discovered and exploited from some tight  
 44 tuff reservoirs, such as the Jatibarang oil and gas field in Indonesia, the Samgori oilfield in the Republic of

45 Georgia, the green tuff oil and gas reservoirs in the Akita and Niigata basins in Japan, the tuff reservoir in  
46 the Qingxi Sag, the tuff reservoir in the Erlian Basin, and the Urho oilfield in the Junggar Basin, China  
47 (Grynberg et al., 1993; Thomas Kalan and Sitorus, 1994; Tomaru et al., 2009; Jiang et al., 2015; Wei et al.,  
48 2018; Wang et al., 2019).

49 Tight tuff reservoirs usually exhibit a series of significant differences from the other tight reservoirs,  
50 such as tight sand and shale (Liang et al., 2014). Tuff is formed from volcanic ash (<2 mm) and shows  
51 tuffaceous texture, which is dominated by fine-grained pyroclastic materials (>90%) (Jiang et al., 2015)  
52 generated in explosive volcanic eruptions, which spread laterally by wind drift over large distances (Kolata  
53 et al., 1987; Huff et al., 1992; Königer et al., 2002; Huff, 2008; Qiu et al., 2014). Sedimentation occurs  
54 when these tuffaceous materials fall directly into a lake, termed “primary airfall type”, or are transported  
55 into a lake by streams or rivers, known as “water carrying type” (Atri et al., 1999; Haaland et al., 2000;  
56 Dunggen et al., 2010; Zhang et al., 2019). Unlike shale oil and gas reservoirs, tuff reservoirs are not  
57 necessarily unconventional reservoirs, which contain both source and reservoir in the same strata. For  
58 example, it was reported that the crude oil in the tuff reservoir of the Tiaohu Formation has been proved to  
59 be from the underlying Lucaogou Formation by oil-source correlation (Ma et al., 2015; Hackley et al.,  
60 2016). Furthermore, tight tuff reservoirs usually exhibit higher porosity than shale reservoirs, and  
61 interparticle pores contribute more to the pore system in tight tuff reservoirs rather than organic matter  
62 pores, which provide the main reservoir space in shale (Zhu et al., 2012; Jiao et al., 2014; Jiang et al., 2015;  
63 Yang et al., 2017; Xu et al., 2018).

64 In recent years, tight oil has been found in the Tiaohu and Haerjiawu Formation tuffs, which are both  
65 “primary airfall type” tuff reservoirs, through many wells drilled in the Santanghu Basin, such as L1, M7,  
66 M56-12H and M58H, which yielded a daily production of approximately 20 m<sup>3</sup> crude oil. Hence, tuff

67 reservoirs have become an important oil reservoir and deserve further research. Some research into the  
68 Tiaohu Formation tuff reservoir has been undertaken, mainly focused on the basic characteristics of  
69 petrologic features, reservoir space, and physical properties (Jiao et al., 2014; Liang et al., 2014; Ma et al.,  
70 2015, 2016). However, a comparative analysis of tuff reservoirs in the Haerjiawu and Tiaohu formations  
71 has not been conducted. Moreover, the formation mechanism of the differences in basic characteristics  
72 between the two sets of tuff reservoirs needs further research. Therefore, the principal objectives of this  
73 study are as follows: (1) to demonstrate the basic petrologic features, reservoir space, and physical  
74 properties of tuff reservoirs in both the Tiaohu and Haerjiawu formations, then determine the differences  
75 between them; and (2) to discuss the formation mechanism of the basic characteristics differences. This  
76 study can provide valuable data for predicting favorable tuff reservoirs in the Santanghu Basin and may  
77 also draw more attention to the value of this special type of reservoir in other regions. Furthermore, as a  
78 special type of tight oil reservoir, it is of important scientific significance to expand the understanding of  
79 this potential unconventional oil and gas exploration and development target.

## 80 **2. Geological setting**

81 The Santanghu Basin is located in the northeast Xinjiang Region, China, and is bordered by Mongolia  
82 to the north, the Turpan-Hami Basin to the south, and the Junggar Basin to the west. As a superimposed  
83 basin that developed over an Early Palaeozoic basement, the Santanghu Basin is sandwiched between the  
84 Tianshan and Altai mountains, and composed of three tectonic units, the NE thrust fold belt, central  
85 depression belt, and SW thrust fold belt (Xu et al., 2013; Liu et al., 2018). The central depression belt  
86 consists of four uplifts (Shitoumei, Chahaquan, Fangfangliang, and Weibei Uplift) and five sags  
87 (Hanshuiquan, Tiaohu, Malang, Naomaohu, and Suluke Sag). The Malang Sag is the most important  
88 secondary structural unit, which covers an area of approximately 1800 km<sup>2</sup> (Fig. 1). Vertically, the strata

99 consist of the Carboniferous (Haerjiawu Formation and Kalagang Formation), Permian (Lucaogou  
100 Formation and Tiaohu Formation), Triassic, Jurassic, Cretaceous, the Palaeogene system, and Quaternary  
101 rocks.

102 Insert [Fig. 1]

103 Volcanic activity occurred during the Carboniferous and Permian. The volcanic eruption cycle  
104 indicates volcanic activity strength and duration. At the early stage of volcanic activity, explosive and  
105 fallout facies were formed from the strong and intensive eruption of solid and plastic ejecta. In the middle  
106 stage of volcanic activity, effusive facies developed from the slowly flowing magma driven by subsequent  
107 ejecta under the influence of gravity. At the late stage, eruptive sedimentary facies were formed from  
108 volcanic ash that fell on land or in lakes after a long-distance transport in the air. Finally, the volcanic  
109 activity entered a short dormant period, during which volcanic sedimentary facies developed from  
110 terrigenous volcaniclastic rock after water transportation. The process from strong eruption, to quiet  
111 overflow, then to tuff deposition and volcanic dormancy is called a cycle of volcanic activity (Hu et al.,  
112 2013; Nyland et al., 2013). An eruption cycle often includes several eruption activities, which are reflected  
113 by sedimentary discontinuities, such as unconformities (Bowman et al., 2019; Yang et al., 2019). During  
114 the Carboniferous, intense volcanism happened in the Malang Sag was caused by the collision of the  
115 Kazakhstan and Siberia plates. Reverse faults were channels for magma, forming multiple volcanic belts.  
116 Tuff, carbonaceous mudstone, tuffaceous mudstone, and oil shale formed during the breaks in the volcanic  
117 eruption. Based on the volcanic activity and lithology characteristics, there are two relatively complete  
118 volcanic eruption cycles in the Haerjiawu Formation (Fig. 2). The lower volcanic eruption cycle comprises  
119 volcanic rock, carbonaceous mudstone, and tuffaceous mudstone. The upper volcanic eruption cycle  
120 comprises volcanic rock, and thin layers of tuffaceous mudstone and tuff. The volcanic activity gradually

111 weakened during the Kalagang Formation. During the Permian Lucaogou Formation deposition, the  
 112 volcanic activity was weak and fine-grained lacustrine sediments, such as mudstones, lime mudstones, and  
 113 dolomitic mudstones, developed widely (Pang et al., 2018; Liu et al., 2018, 2019; Zhang et al., 2019).  
 114 However, the volcanic activity was more prevalent during the early deposition of the Tiaohu Formation  
 115 (Zhu et al., 2005), which displays a complete volcanic eruption cycle, during which basalt of effusive  
 116 facies developed at the bottom of the formation, tuff of eruptive facies developed in the middle, and  
 117 mudstone and tuffaceous mudstone developed at the top.

118 Insert [Fig. 2]

### 119 **3. Samples, Data and Experimental method**

#### 120 **3.1. Sample Collection and Published Data Sources**

121 A total of 22 samples from the Haerjiawu Formation were collected from the cores of wells in the  
 122 Malang Sag for the examination of reservoir characteristics. Sixteen core plugs samples ( $2.5 \times 5.0$  cm) of  
 123 the Haerjiawu Formation parallel to the bedding plane were selected to test the porosity and permeability,  
 124 and another six samples were assigned to X-ray diffraction (XRD) analysis for mineral composition. All  
 125 the mineral composition data of the Tiaohu Formation samples were collected from Jiao et al. (2014) and  
 126 Ma et al. (2016), although the core, rock thin section, and scanning electron microscope (SEM)  
 127 observations for these samples were newly conducted in this research. Furthermore, a total of 24 samples  
 128 from the Tiaohu Formation were used to test the porosity and, permeability, and the porosity data of seven  
 129 samples were collected from Jiao et al. (2014) and Ma et al. (2016). Four samples from the Haerjiawu  
 130 Formation were used in elemental analysis, and all elemental data for the Tiaohu Formation samples were  
 131 collected from Ma et al. (2016).

132 **3.2. Experiments analytical methods**

133 Analyses including rock thin section observation, scanning electron microscope (SEM) observations,  
134 and porosity and permeability tests of the tuffs were conducted at the State Key Laboratory of Petroleum  
135 Resource and Prospecting and the National Key Lab of Heavy Oil Processing. X-ray diffraction (XRD)  
136 experiments and elemental analyses were completed at the Micro Structure Analytical Lab of Peking  
137 University.

138 Petrographic thin sections of the core samples were observed under plane-polarized light and  
139 orthogonal polarized light with a polarizing microscope. The CL8200 MK5-2 optical cathodoluminescence  
140 system was applied at room temperature to identify the mineral composition and size distribution. The thin  
141 sections were placed under vacuum before cathode rays were emitted. The images were obtained by a  
142 Leica Camera System when the vacuum was <0.5 mB. Small samples of massive tuff were selected, and  
143 their fresh surfaces were coated with gold for SEM observation using a high-resolution field emission  
144 SEM system (FEI Quanta200). Some samples were Ar-ion polished by secondary electron beam before  
145 SEM observation. The tuff core samples were crushed into <40 µm diameter powder, and then the mineral  
146 compositions were determined by XRD analysis using a Rigaku automated powder diffractometer  
147 (D/MAX-RA) equipped with a Cu X-ray source (40 Kv, 100 mA) with the scanning range of 3°–70°,  
148 sampling step size of 0.01°, and scanning speed of 4°/min. Minerals were recognized according to the  
149 diffractogram, and their relative abundances values (weight percentages) were analyzed  
150 semi-quantitatively.

151 The major and trace elements in the tuffs were measured using X-ray fluorescence (XRF) and  
152 Inductively Coupled Plasma-Atomic Emission Spectrometry (ICP-AES) (PerkinElmer Optima 8300  
153 Series), respectively. Porosity and permeability were tested under atmospheric pressure conditions using

154 helium and nitrogen, respectively. The pore throat radii of the tuffs were determined using a high-pressure  
 155 mercury injection meter (Pore Master GT60). Tuff samples were treated in an oil-wash of methylbenzene  
 156 and ethyl alcohol prior to testing to eliminate the effect of oil on porosity and permeability measurements.

157 **4. Results**

158 **4.1. Petrographic Thin Section Observation**

159 The Permian Tiaohu Formation tuff reservoir in the Santanghu Basin mainly consists of vitric  
 160 fragments, and contains a small proportion of crystal and lithic tuff. The tuffs are characterized by an  
 161 earthy yellow colour and massive bedding (Figs. 3a and 3b). The vitric fragments exhibit a high degree of  
 162 alteration from the primitive volcanic ash, and the crystals exhibit obvious extinction phenomenon under  
 163 cross-polarized light (Figs. 3c and 3d). The crystal fragments are larger in size and characterized in stripes  
 164 with directional arrangement (Figs. 3e and 3f). The formation temperature of some authigenic minerals can  
 165 be reflected by the cathodoluminescence. For example, under cathodoluminescence, quartz formed at high  
 166 ( $>573^{\circ}\text{C}$ ), medium-high ( $300^{\circ}\text{C}$ – $573^{\circ}\text{C}$ ), and low ( $<300^{\circ}\text{C}$ ) temperatures appears bluish-purple,  
 167 brownish-red, and non-luminescent, respectively. In contrast, calcite is orange and feldspar emits variable  
 168 light (Zhang et al., 2003; Wark et al., 2007; Liu et al., 2018). Most quartz grains in the vitric tuffs of the  
 169 Tiaohu Formation are non-luminescent under cathodoluminescence (Figs. 3g and 3h), which indicates an  
 170 authigenic product during low temperature diagenesis. The quartz content is the highest (40%–70%)  
 171 among all the mineral types, followed by albite (10%–40%) (Table 1). However, the clay content is low  
 172 (<10%) and the clay minerals are formed by diagenesis rather than originating detrital input, and are  
 173 mainly dispersed among authigenic quartz and feldspar minerals (Fig. 3i).

174 Insert [Fig. 3]

175 Insert [Table 1]

176 In contrast, tuff in the Carboniferous Haerjiawu Formation consists of crystal fragments and detritus  
 177 (Figs. 4a and 4b). There are both luminescent and non-luminescent quartz grains under  
 178 cathodoluminescence (Figs. 4c~f), which indicates two sources for quartz, authigenic quartz formed during  
 179 diagenesis and detrital quartz from igneous parent rock. The feldspar content is the highest (10%–50%),  
 180 followed by quartz (10%–40%), which is different from the mineral composition of the Permian Tiaohu  
 181 formation (Table 1). And the feldspar is mainly anorthite. The overall content of clay minerals is low  
 182 (<20%). The content of calcite and zeolite ranges from 10%–50%.

183 Insert [Fig. 4]

184

## 185 **4.2. Reservoir space**

### 186 **4.2.1. The Tiaohu Formation**

187 Reservoir space in the Tiaohu Formation mainly consists of various pores types, including  
 188 interparticle, intraparticle, and organic matter pores, as well as structural fractures, especially high-angle  
 189 fractures. The well-developed micropores are difficult to observe directly in thin section, but can be easily  
 190 observed through scanning electron microscope (SEM) (Figs. 5a~f). The cracks and micro fractures can be  
 191 directly observed in core samples and thin sections (Figs. 5g and 5h). Pore size is mainly on the  
 192 micron–nanometer scale, and can be divided into three types according to the classification in Loucks et al.  
 193 (2012) and Zhao et al. (2013): (1) interparticle pores between minerals, such as quartz and feldspar; (2)  
 194 intraparticle pores within minerals, such as feldspar; and (3) organic matter pores.

195 Insert [Fig. 5]

196

#### 197 **(1) Interparticle pores**

198        The interparticle pores can be clearly and easily observed in the Tiaohu Formation tuffs, especially the  
 199        vitric tuff. These pores mainly distribute among the major mineral components of quartz and feldspar (Fig.  
 200        5b).

201        **(2) Intraparticle pores**

202        Intraparticle pores in the Tiaohu Formation tuffs mainly consist of dissolution pores within feldspars,  
 203        intercrystalline pores within pyrite framboids, and pores within the clay minerals. Dissolution intraparticle  
 204        pores commonly develop within feldspar grains (Fig. 5c), which can be identified by the elemental  
 205        composition (O, Si, Al, and Na) measured by energy dispersive spectrometer analysis. Pyrite framboids  
 206        widely develop in the tuff, and consist of many pyrite crystals, among which many micropores appear (Fig.  
 207        5d). The main clay mineral is chlorite, which is in the form of cleavage-sheet shapes with micropores  
 208        developed among them (Fig. 5e).

209        **(3) Organic matter pores**

210        The organic matter pores of various shapes in tuff can be recognized in Ar-ion polished samples  
 211        through SEM observation. These pores are generally <1.0 μm and can act as storage space in the  
 212        organic-matter-bearing tuff reservoir (Fig. 5f). However, organic matter pores are not widely developed in  
 213        the study area samples because of relatively low thermal maturity (Jiao et al., 2014; Meng et al., 2014),  
 214        which indicates a probably limited contribution of organic matter pores to the effective pore network.

215        Fractures can have a significant effect on hydraulic fracturing and hydrocarbon production (Gale et al.,  
 216        2007; Loucks et al., 2012). In the tuff core samples, many structural fractures, generally the high-angle  
 217        fractures cemented by calcite, can be widely observed. Residual oil is easily observed in these fractures,  
 218        indicating that they are important pathways for hydrocarbon migration (Fig. 5g). In fact, a large abundance  
 219        of oil accumulated in the volcanic rocks of the Permian Tiaohu Formation has also been shown to have

220 migrated from the source rock in the second member of the underlying Lucaogou Formation (Ma et al.,  
 221 2015; Hackley et al., 2016). In addition, micro fractures can also be observed under the microscope (Fig.  
 222 5h).

#### 223 **4.2.2. The Haerjiawu Formation**

224 Reservoir space in the Haerjiawu Formation is mainly composed of interparticle pores and fractures.  
 225 Some different-sized oval, polygonal, and irregular interparticle (Fig. 6a) and gas pores (Fig. 6b), are  
 226 primary pores, which remain after consolidation and compaction of pyroclastic particles during diagenesis.  
 227 Primary gas pores are round or oval in different sizes (0.1–0.3 mm), and mainly distribute in the detritus.  
 228 Gas pores were formed when the gas entrained in the magma was not released immediately. Some  
 229 interparticle pores distribute among authigenic quartz and feldspars. These interparticle pores were formed  
 230 with the formation of authigenic minerals and mineral dissolution rather than as residual during diagenesis  
 231 process (Fig. 6c~g). Primary contraction fractures and secondary structural fractures are the two types of  
 232 fractures in the tuff of the Haerjiawu Formation. Contraction fractures are formed by the uneven internal  
 233 stress and differential contraction during rapid cooling of high temperature magma (Xu et al., 2013; Liang  
 234 et al., 2014; Masotta et al., 2020). The shape of contraction fractures is very irregular, primarily occurring  
 235 as mesh, caudate, or cracks (Fig. 6h). Structural fractures formed under northeast to southwest oriented  
 236 tectonic stress present at the end of the Palaeozoic Era, and became more complex after the superposition  
 237 of a series of later tectonic movements (Li et al., 2013). There are many structural fractures characterized  
 238 by a variety of widths and lengths, variably filling with secondary minerals such as calcite and zeolite (Fig.  
 239 6i).

240 Insert [Fig. 6]

241

242 **4.3. Reservoir physical properties**

243 Physical properties of the tuff directly controlled the reservoir storage capacity. The physical property  
 244 data of 31 tuff samples from the Tiaohu Formation show that the tuff reservoir is characterized by  
 245 relatively high porosity, mainly between 15% and 25% (Fig. 7, Table 2). However, the permeability is  
 246 relatively low, mostly from 0.01–0.10 mD under atmospheric pressure conditions (Fig. 7). The physical  
 247 property data of sixteen tuff samples from the Haerjiawu Formation show that the reservoir is characterized  
 248 by both low porosity (mainly <10%; Fig. 7) and low permeability (under atmospheric pressure conditions,  
 249 mainly <0.1 mD; Fig. 7).

250 Insert [Fig. 7]

251 Insert [Table 2]

252

253 **5. Discussion**254 **5.1. Differences in tuff reservoir characteristics**255 **5.1.1. Nature of tuff**

256 The crystal pyroclasts in the Tiaohu Formation tuffs are chiefly quartz and albite. The composition  
 257 of vitric pyroclasts is largely felsic, which is mainly composed of Si and O elements, followed by Al, Na,  
 258 and K. The mineral and elemental composition characteristics indicate an origin from acidic or  
 259 intermediate-acid volcanic ash (Ma et al., 2016). However, the crystal pyroclasts in the Haerjiawu  
 260 Formation mainly consist of feldspar, and the quartz content is low. Furthermore, the type of feldspar in the  
 261 Haerjiawu Formation is mainly anorthite, which indicates a primary origin of basic volcanic ash, and is  
 262 supported by the major and trace element (Fig. 8).

263 Insert [Fig. 8]

264 **5.1.2. Origin of tuff**

265 Tuffs in the Tiaohu Formation are mainly vitric tuffs with pure compositions and fewer crystal  
 266 fragments or detritus. Tuffs in the Haerjiawu Formation are mainly crystal tuffs and lithic tuffs. The types  
 267 of tuff varied with distance from the volcanic source because the original material changed during the  
 268 volcanic eruption (Ma et al., 2016). Vitric tuff is commonly distributed far from the volcano, while crystal  
 269 tuff and lithic tuff appear near the volcanic orifice. The volcanism was frequent during the Carboniferous,  
 270 and there were many volcanic craters in the basin; therefore, crystal tuff and lithic tuff are widely  
 271 distributed. The intermediate-acidic tuff formed at the end of a volcanic eruption cycle in the Tiaohu  
 272 Formation is distributed above a set of stable mafic–intermediate volcanic rocks. These tuffs represent the  
 273 evolution from basic magma to acidic magma along with the decreasing intensity of volcanic activity  
 274 (Howells et al., 1986; Wang et al., 2006). The volcanism period was extensive and prolonged, forming  
 275 large-scale thick vitric tuff.

276 **5.2. Cause of the tuff micropores formation**277 **5.2.1. Alteration**

278 Most of the interparticle pores in both formations were formed from alteration, and can be regarded as  
 279 alteration pores. Alteration pores can significantly improve the quality of hydrocarbon reservoirs, because  
 280 alteration is an important volume reduction process as diagenetic products are volumetrically compacted  
 281 compared with the parent material (Rowe et al., 2012; Zhu et al., 2014; Liu et al., 2019). Alteration  
 282 occurred continuously from the beginning of deposition because of the instability of volcanic glasses in the  
 283 Tiaohu and Haerjiawu tuff.

284 The alteration of volcanic ash comprises a series of geochemical processes, such as vitreous  
 285 dissolution, migration, precipitation, recrystallization, and alteration to clay minerals (McHenry, 2009;

286 Kirov et al., 2011; Sell et al., 2015; Hong et al., 2019). The formation of authigenic minerals is  
 287 accompanied by volume decreases, and the formation of numerous micropores within the authigenic  
 288 minerals. Quartz is the most important alteration product, and there is a clearly positive relationship  
 289 between the content of quartz and the porosity of tuff (Fig. 9).

290 Insert [Fig. 9]

291 The alteration of glass is affected by various geological factors, such as temperature, pressure, pH,  
 292 and fluid composition (Gíslason and Oelkers, 2003; Wolff et al., 2004; Aradóttir et al., 2013; Declercq et  
 293 al., 2013; Andersen et al., 2018; Minde et al., 2018; Andersen and Berawala, 2019). The dissolution rates  
 294 of glassy basalt and rhyolite decreased dramatically with the increase in pH under acidic conditions,  
 295 minimized at near-neutral pH, and then slowly increased with increasing pH when it was under alkaline  
 296 conditions. All other factors display similar effects as temperature, wherein the higher the temperature was,  
 297 the faster the dissolution rate was. During diagenesis, temperature increased and acid was released from  
 298 organic matter thermal maturation, which reached the requirements for the dissolution of natural  
 299 alumino-silicate volcanic glasses, the removal of metals elements from the glass structure via proton  
 300 exchange reactions, and the precipitation of silica (and therefore alteration) (Declercq et al., 2013; Liu et  
 301 al., 2019).

302 The Tiaohu Formation tuff physical properties are better than the Haerjiawu Formation tuff  
 303 properties, in part because the intermediate-acidic volcanic ash is more easily altered than basic volcanic  
 304 ash. The high SiO<sub>2</sub> content leads to high content of Si-O tetrahedra in the acidic magma. Because the  
 305 effective static charges of oxygen decrease and the attraction capacity of the cationic decreases, Si-O and  
 306 Al-O are easier to separate from the original glass than other compounds to form minerals such as quartz  
 307 and feldspar (Tsukamoto et al., 2003; Agangi et al., 2011; Azer et al., 2019; Liu et al., 2019). Furthermore,

308 fewer interparticle pores formed by alteration in the crystal tuff and lithic tuff than in vitric tuff under the  
309 same geological conditions, because alteration only occurs in the vitreous textures of volcanic material  
310 components. Therefore, the alteration degree of the Tiaohu tuff is much higher, and its physical properties  
311 are better than that of Haerjiawu Formation.

312 The dissolution of volcanic glass, as one of the methods of alteration, is dramatically controlled by the  
313 pH of fluid conditions in reservoir (Gíslason and Oelkers, 2003; Wolff et al., 2004; Aradóttir et al., 2013;  
314 Declercq et al., 2013). Hence, a certain amount of sedimentary organic matter in the Tiaohu Formation  
315 tuffs is favourable for a high degree of alteration, because organic acids released during the thermal  
316 maturation would promote the dissolution of volcanic glass. The Tiaohu Formation tuffs are overlain by a  
317 set of stable mudstones, from which some of the organic acids in the Tiaohu Formation originated.

318 The impact of temperature on the alteration of tuff is reflected in two aspects: the impact on the  
319 generation of organic acids as organic matter thermal evolution affected by temperature and the impact on  
320 the alteration rate as the temperature increases. Significant quantities of organic acids would be generated  
321 and released when the diagenetic temperature was at approximately 60 °C (MacGowan and Surdam, 1988).

322 The content of organic acids would increase until the temperature exceeded the preservation range of  
323 organic acids (80 °C–120 °C). When the temperature rose to 120 °C–160 °C, the concentration of CO<sub>2</sub>  
324 would increase rapidly, but the concentration of organic acids would decrease because of the  
325 decarboxylation conversion of dicarboxylic acid to monocarboxylic acid (Surdam et al., 1984, 1989;  
326 Manning et al., 1994). The burial history of the Malang Sag suggests that the Tiaohu Formation reached its  
327 maximum palaeoburial depth during the Late Cretaceous (Zhao et al., 2003). The thermal history suggests  
328 that the Tiaohu Formation tuff reached approximately 60 °C in the Early Cretaceous and the hottest  
329 geothermal conditions (90 °C–100 °C) during the Late Cretaceous.

330 Altogether, the alteration of volcanic glass, which is the parent material of vitric fragments, displays  
 331 an important effect on the characteristics of high porosity and low permeability in the tuff. This  
 332 phenomenon also appears in the Lucaogou Formation below the Tiaohu Formation (Liu et al., 2019).  
 333 Individual interparticle pores formed during alteration within the tuff have small sizes but are high in  
 334 number, which results in relatively high porosity. The pore throat radii of the Tiaohu tuff are generally <1.0  
 335 μm (mostly <0.1 μm) (Fig. 10). Given a positive correlation between permeability and pore throat radius  
 336 (Fig. 10), the fine granularity and small pore throat radii of the tuff results in a very low permeability. In  
 337 fact, alteration occurs where the vitric fragments distribute, and the vitric fragments are always surrounded  
 338 tightly by clay minerals (Fig. 6c and 6d); thus, the pores formed during alteration are isolated by clay  
 339 minerals, which is the primary reason for small pore throat radii. The Haerjiawu tuff reservoir contains  
 340 relatively more clay minerals than the Tiaohu Formation tuff reservoir, which indicates relatively lower  
 341 permeability.

342 Insert [Fig. 10]

### 343 **5.2.2. Organic matter related pores**

344 The organic acid released during organic matter thermal maturation displays stronger solubility than  
 345 inorganic acid, and not only accelerates vitric fragments alteration, but also corrodes the crystal fragments  
 346 and detrital minerals to form dissolution pores (Hower et al., 1976; Espitalie et al., 1980; Meshiri, 1986;  
 347 Barth and Bjørlykke, 1993; Gislason and Oelkers, 2003; Wang et al., 2006; Liu et al., 2019) (Fig. 5c).  
 348 Hence, dissolution micropores are an important contribution to the pore system in tuff reservoirs. Pyrite  
 349 framboids occur in the Tiaohu Formation tuff reservoir with interparticle pores. The formation of pyrite  
 350 framboids is closely related to organic matter decomposition and P, S, and Fe cycles (Chowdhury and  
 351 Noble, 1996; Kalatha and Economou-Eliopoulos, 2015; Yuan et al., 2017). Occasionally, kerogen infilled

352 in pyrite framboids develops organic pores. Furthermore, organic matter pores formed because of  
 353 hydrocarbon generation and excretion during organic matter thermal maturation are another contribution to  
 354 pore systems in the Tiaohu Formation tuff reservoir. However, pyrite framboids and organic matter are not  
 355 observed in samples of the Haerjiawu tuff reservoir, which is another reason of its relatively lower  
 356 porosity.

357 **5.2.3. Compaction**

358 Under the load of overlying water or sediments, the water in the Haerjiawu and Tiaohu formation tuff  
 359 reservoirs is drained constantly and the volume is compressed in the loose sediments, so the primary  
 360 porosity of the reservoirs reduces gradually. Therefore, the total porosity was high at the early stage of  
 361 sediment formation, and then reduced significantly by compaction during diagenesis (Goult et al., 2016;  
 362 Liu et al., 2019). However, due to the alteration of volcanic glass, the total porosity would increase during  
 363 a certain stage of the diagenetic process. Hence, the total porosity of tuffs can be calculated by adding the  
 364 compaction residual porosity and the porosity produced during alteration. Because of the competing effects  
 365 of compaction and alteration, the porosity of the tuff may show no obvious changes with the increase in the  
 366 depth.

367 Three stages can be recognized for the evolution of tuff porosity: porosity reducing stage caused by  
 368 normal compaction, porosity increasing stage caused by alteration, and invariable porosity stage after  
 369 tectonic uplift because of diagenetic irreversibility. According to the burial history and thermal evolution  
 370 history, the three stages occurred before the Early Cretaceous, between the Early Cretaceous and Late  
 371 Cretaceous, and after the Late Cretaceous, respectively (Fig. 11).

372 Insert [Fig. 11]

373 The compaction process dominated during the porosity reducing stage before the Early Cretaceous,

374 while the alteration process dominated during the porosity increasing stage. For the same type of tuff, the  
 375 porosity increased by alteration was greater than that reduced by compaction, and the total porosity  
 376 increased during the porosity increasing stage. However, when the burial depth was too large, compaction  
 377 dominated, and the porosity of the tuff decreased with the increase in burial depth. The Haerjiawu  
 378 Formation tuff reservoir is much deeper than the Tiaohu Formation, and the porosity of the Haerjiawu  
 379 Formation is smaller than that of the Tiaohu Formation indicating that greater burial depth is another main  
 380 reason besides the influence of the weak alteration caused by volcanic ash.

381 In addition, it can be seen from the plot of depth and porosity that both the Haerjiawu and Tiaohu  
 382 formation samples show a decrease in porosity with the increase in burial depth, followed by porosity  
 383 increases because of alteration (Fig. 12). The Tiaohu Formation samples show larger porosity than those of  
 384 Haerjiawu Formation samples in general because of higher alteration degree. However, the Haerjiawu  
 385 Formation samples exhibit much lower porosity when the burial depth is larger than 2900m because of  
 386 compaction dominating at much larger burial depth.

387 Insert [Fig. 12]

## 388 **6. Conclusions**

389 The tuff reservoir in the Tiaohu Formation mainly consists of vitric tuff with low amounts crystal  
 390 fragments or detritus. Pores in tuffs are mainly interparticle pores among quartz and feldspar minerals. The  
 391 tuff exhibits the characteristics of high porosity (10%–25%) and low permeability (mainly 0.01–0.50 mD).  
 392 However, the tuff reservoir in the Haerjiawu Formation exhibits high crystal fragment content. Primary  
 393 pores and alteration pores are the main pore types. The tuff reservoir is characterized by low porosity  
 394 (<10%) and low permeability (mainly <0.1 mD).

395 Alteration of volcanic glasses or ashes was the principal mechanism of micropore formation in tuff

396 reservoirs. Individual interparticle pores formed during alteration within the tuff have small sizes but are  
397 large in number, which results the high overall porosity of the Tiaohu tuff. The organic matter also  
398 contributes substantially to the high porosity. However, compaction is destructive to the pores formation.  
399 The acid nature of original volcanic ash, the type of vitric tuff, and the shallow burial depth for the tuff in  
400 the Tiaohu Formation are the main reasons of the better physical properties than those of tuff in the  
401 Haerjiawu Formation.

402

#### 403 **AUTHOR INFORMATION**

404 Corresponding author

405 \*E-mail: [202majian@163.com](mailto:202majian@163.com); liuguoheng123@yeah.net.

406

#### 407 **Author Contributions**

408 The manuscript was written through contributions of all authors. All authors have given approval to the  
409 final version of the manuscript.

410

#### 411 **Notes**

412 The authors declare no competing financial interest.

413

#### 414 **ACKNOWLEDGEMENTS**

415 This research was supported financially by the National Natural Science Foundation of China (No.:  
416 41472111) and the China Postdoctoral Science Foundation (No.: 2017M611109). The authors thank the  
417 PetroChina Turpan-Hami Oilfield Company for providing valuable geological data, as well as the crude oil

418 and core samples.

419

420 **REFERENCES**

- 421 Agangi, A., McPhie, J., Kamenetsky, V.S., 2011. Magma chamber dynamics in a silicic LIP revealed by  
422 quartz: The Mesoproterozoic Gawler Range Volcanics. *Lithos* 126(1-2), 68-83.
- 423 Andersen, P.Ø., Wang, W., Madland, M.V., Zimmermann, U., Korsnes, R.I., Bertolino, S.R.A., Minde, M.,  
424 Schulz, B., Gilbricht, S., 2018. Comparative study of five outcrop chalks flooded at reservoir  
425 conditions: chemo-mechanical behaviour and profiles of compositional alteration. *Transp Porous Med*  
426 121, 135-181.
- 427 Andersen, P.Ø., & Berawala, D.S. (2019, August 1). Modeling of Creep-Compacting Outcrop Chalks  
428 Injected with Ca-Mg-Na-Cl Brines at Reservoir Conditions. Society of Petroleum Engineers.  
429 doi:10.2118/192018-PA.
- 430 Aradóttir, E.S.P., Sigfússon, B., Sonnenthal, E.L., Björnsson, G., Jónsson, H., 2013. Dynamics of basaltic  
431 glass dissolution–capturing microscopic effects in continuum scale models. *Geochimica et*  
432 *Cosmochimica Acta* 121, 311-327.
- 433 Atri, A.D., Pierre, F.D., Lanza, R., Ruffini, R., 1999. Distinguishing primary and resedimented vitric  
434 volcaniclastic layers in the Burdigalian carbonate shelf deposits in Monferrato (NW Italy).  
435 *Sedimentary Geology* 129, 143-163.
- 436 Azer, M.K. Gahlan, H.A. Asimow, P.D. Al-Kahtany, K.M., 2019. The common origin and alteration history  
437 of the hypabyssal and volcanic phases of the Wadi Tarr albite complex, southern Sinai, Egypt. *Lithos*  
438 324-325, 821-841.
- 439 Barth, T., Bjørlykke, K., 1993. Organic acids from source rock maturation: generation potentials, transport

- 440 mechanisms and relevance for mineral diagenesis. *Applied Geochemistry* 8, 325-337.
- 441 Bowman, N.H., Van Otterloo, J., Cairns, C.P., Taylor, D.H., Cas, R.A.F., 2019. Complex evolution of  
442 volcanic arcs: The lithofacies and palaeogeography of the Cambrian Stavely Arc, Delamerian Fold  
443 Belt, Western Victoria. *Journal of Volcanology and Geothermal Research* 373, 120-132.
- 444 Cao, Z., Liu, G.D., Kong, Y.H., Wang, C.Y., Niu, Z.C., Zhang, J.Y., Geng, C.B., Shan, X., Wei, Z.P., 2016.  
445 Lacustrine tight oil accumulation characteristics: Permian Lucaogou Formation in Jimusaer Sag,  
446 Junggar Basin. *International Journal of Coal Geology* 153, 37-51.
- 447 Chowdhury, A.H., Noble, J.P.A., 1996. Organic carbon and pyrite sulphur relationships as evidences of  
448 bottom water conditions of sedimentation, Albert Formation fine-grained lacustrine sediments, New  
449 Brunswick, Canada. *Marine and Petroleum Geology*, 13(1), 79-90.
- 450 Cui, J.W., Li, S., Mao, Z.G., 2019. Oil-bearing heterogeneity and threshold of tight sandstone reservoirs: A  
451 case study on Triassic Chang7 member, Ordos Basin. *Marine and Petroleum Geology* 104, 180-189.
- 452 Declercq, J., Diedrich, T., Perrot, M., Gislason, S.R., Oelkers, E.H., 2013. Experimental determination of  
453 rhyolitic glass dissolution rates at 40-200 °C and  $2 < \text{pH} < 10.1$ . *Geochimica et Cosmochimica Acta*  
454 100, 251-263.
- 455 Dunggen, S., Olgun, N., Croot, P., 2010. The role of airborne volcanic ash for the surface ocean  
456 biogeochemical iron-cycle: A review. *Biogeosciences* 7, 827-844.
- 457 Flewelling, S.A., Tymchak, M.P., Warpinski, N., 2013. Hydraulic fracture height limits and fault  
458 interactions in tight oil and gas formations. *Geophysical Research Letters* 40, 3602-3606.
- 459 Gale, J.F., Reed, R.M., Holder, J., 2007. Natural fractures in the Barnett Shale and their importance for  
460 hydraulic fracture treatments. *AAPG Bulletin* 91, 603-622.
- 461 Gíslason, S.R., Oelkers, E.H., 2003. Mechanism, rates and consequences of basaltic glass dissolution: An

- 462 experimental study of the dissolution rates of basaltic glass as a function of pH and temperature.
- 463 *Geochimica et Cosmochimica Acta* 67, 3817-3832.
- 464 Goultby, N.R., Sargent, C., Andras, P., Aplin, A.C., 2016. Compaction of diagenetically altered mudstones –  
465 Part 1: Mechanical and chemical contributions. *Marine and Petroleum Geology* 77, 703-713.
- 466 Grynberg, M.E., Papava, D., Shengelia, M., Takaishvili, A., Nanadze, A., Patton, D.K., 1993. Petrophysical  
467 characteristics of the middle Ecoene laumontite tuff reservoir, Samgori Field, Republic of Georgia.
- 468 *Journal of Petroleum Geology* 16, 313-322.
- 469 Haaland, H.J., Furnes, H., Martinsen, O.J., 2000. Paleogene tuffaceous intervals, Grane Field (Block  
470 25/11), Norwegian North Sea: their depositional, petrographical, geochemical character and regional  
471 implications. *Marine and Petroleum Geology* 17, 101-118.
- 472 Hackley, P.C., Fishman, N., Wu, T., Baugher, G., 2016. Organic petrology and geochemistry of mudrocks  
473 from the lacustrine Lucaogou Formation, Santanghu Basin, northwest China: Application to Lake  
474 Basin evolution. *International Journal of Coal Geology* 168, 20-34.
- 475 Hong, H.L., Zhao, L.L., Fang, Q., Algeo, T.J., Wang, C.W., Yu, J.X., Gong, N.N., Yin, K., Ji, K.P., 2019.  
476 Volcanic sources and diagenetic alteration of Permian-Triassic boundary K-bentonites in Guizhou  
477 Province, South China. *Palaeogeography, Palaeoclimatology, Palaeoecology* 519, 141-153.
- 478 Hu, Z.H., Shen, C.S., Liu, Z.B., 2013. The research method and application of the volcanic rock eruption  
479 cycle and stage in the Bohai Bay Basin. *Petroleum Geophysics* 11(2), 30-33.
- 480 Huff, W.D., 2008. Ordovician K-bentonites: issues in interpreting and correlating ancient tephras.  
481 *Quaternary International* 178, 276-287.
- 482 Huff, W.D., Bergström, S.M., Kolata, D.R., 1992. Gigantic Ordovician volcanic ash fall in North America  
483 and Europe: biological, tectonomagmatic, and event stratigraphic significance. *Geology* 20, 875-878.

- 484 Jiang, Y.Q., Liu, Y.Q., Yang, Z., Nan, Y., Wang, R., Zhou, P., Yang, Y.J., Kou, J.Y., Zhou, N.C., 2015.
- 485 Characteristics and origin of tuff-type tight oil in Jimusar depression, Junggar Basin, NW China.
- 486 Petroleum Exploration and Development 42(6), 741-749.
- 487 Jiao, L.X., Liu, J.T., Zhang, H., Feng, T.Q., Wu, C., Zhang, Q., Guo, K.C., 2014. Tight reservoir
- 488 characteristics and formation conditions of tuff in Santanghu Basin. Natural Gas Geoscience 25(11),
- 489 1697-1705 (in Chinese with English abstract).
- 490 Kalatha, S., Economou-Eliopoulos, M., 2015. Framboidal pyrite and bacterio-morphic goethite at
- 491 transitional zones between Fe–Ni-laterites and limestones: Evidence from Lokris, Greece. Ore
- 492 Geology Reviews 65, 413-425.
- 493 Kirov, G., Samajova, E., Nedialkov, R., 2011. Alteration processes and products of acid pyroclastic rocks in
- 494 Bulgaria and Slovakia. Clay Minerals 46, 279-294.
- 495 Kolata, D.R., Frost, J.K., Huff, W.D., 1987. Chemical correlation of K-bentonite beds in the Middle
- 496 Ordovician Decorah subgroup, upper Mississippi valley. Geology 15, 208-211.
- 497 Königer, S., Lorenz, V., Stollhofen, H., Armstrong, R.A., 2002. Origin, age and stratigraphic significance
- 498 of distal fallout ash tuffs from the Carboniferous-Permian continental Saar-Nahe basin (SW Germany).
- 499 International Journal of Earth Sciences 91, 341-356.
- 500 Kuhn, P. P., di Primio, R., Hill, R., Lawrence, J. R., Horsfield, B., 2012. Three-dimensional modeling study
- 501 of the low-permeability petroleum system of the Bakken Formation. AAPG Bulletin 96, 1867-1897.
- 502 Le Bas, M. J., Le Maitre, R. W., Streckeisen, A., Zanettin, B., 1986. A chemical classification of volcanic
- 503 rocks based on the total alkali-silica diagram. Journal of Petrology 27, 745-750.
- 504 Li, W., Liu, Y.Q., Dong, Y.P., Zhou, X.H., Liu, X.M., Li, H., Fan, T.T., Zhou, D.W., Xu, X.Y., Chen, J.,
- 505 2013. The geochemical characteristics, geochronology and tectonic significance of the Carboniferous

- 506 volcanic rocks of the Santanghu area in northeastern Xinjiang, China. *Science China Earth Sciences*
- 507 56(8), 1318-1333.
- 508 Liang, H., Li, X.N., Ma, Q., Xiang, H., Luo, Q.S., Chen, X., Bai, G.J., Zhang, Q., Meng, Y.L., 2014.
- 509 Geological features and exploration potential of Permian Tiaohu Formation tight oil, Santanghu Basin,
- 510 NW China. *Petroleum Exploration and Development* 41(5), 616-627.
- 511 Liu, G.H., Huang, Z.L., Jiang, Z.X., Chen, J.F., Chen, F.R., Xing, J.Y., 2016. Gas adsorption capacity
- 512 calculation limitation due to methane adsorption in low thermal maturity shale: A case study from the
- 513 Yanchang Formation, Ordos Basin. *Journal of Natural Gas Science and Engineering* 30, 106-118.
- 514 Liu G.H., Liu B., Huang, Z.L., Chen Z.Y., Jiang Z.X., Guo X.B., Li T.W., Chen L., 2018. Hydrocarbon
- 515 distribution pattern and logging identification in lacustrine fine-grained sedimentary rocks of the
- 516 Permian Lucaogou Formation from the Santanghu basin. *Fuel* 222, 207-231.
- 517 Liu, G.H., Zhai, G.Y., Huang, Z.L., Zou, C.N., Xia, X.H., Shi, D.S., Zhou, Z., Zhang, C., Chen, R., Yu, S.F.,
- 518 Chen, L., Zhang, S.H., 2019. The effect of tuffaceous material on characteristics of different
- 519 lithofacies: A case study on Lucaogou Formation fine-grained sedimentary rocks in Santanghu Basin.
- 520 *Journal of Petroleum Science and Engineering* 179, 355-377.
- 521 Liu, Y.M., Ma, K., Hou, J.G., Yan, L., Chen, F.L., 2019. Diagenetic controls on the quality of the Middle
- 522 Permian Lucaogou Formation tight reservoir, southeastern Junggar Basin, northwestern China.
- 523 *Journal of Asian Earth Sciences* 178, 139-155.
- 524 Loucks, R.G., Reed, R.M., Ruppel, S.C., Hammes, U., 2012. Spectrum of pore types and networks in
- 525 mudrocks and a descriptive classification for matrix-related mudrock pores. *AAPG Bulletin* 96,
- 526 1071-1098.
- 527 Ma, J., Huang, Z.L., Gao X.Y., Chen, C.C., 2015. Oil-source rock correlation for tight oil in tuffaceous

- 528 reservoirs in the Permian Tiaohu Formation, Santanghu Basin, northwest China. Canadian Journal of  
529 Earth Sciences 52, 1014-1026.
- 530 Ma, J., Huang, Z.L., Liang, S.J., Liu, Z.Z., Liang, H., 2016. Geochemical and tight reservoir characteristics  
531 of sedimentary organic-matter-bearing tuff from the Permian Tiaohu Formation in the Santanghu  
532 Basin, Northwest China. Marine and Petroleum Geology 73, 405-418.
- 533 Ma, Q.Z., Yang, S.L., Lv, D.P., Wang, M.B., Chen, J.X., Kou, G., Yang, L., 2019. Experimental  
534 investigation on the influence factors and oil production distribution in different pore sizes during  
535 CO<sub>2</sub> huff-n-puff in an ultra-high-pressure tight oil reservoir. Journal of Petroleum Science and  
536 Engineering 178, 1155-1163.
- 537 MacGowan, D.B., Surdam, R.C., 1988. Difunctional carboxylic acid anions in oilfield waters. Organic  
538 Geochemistry 12, 245-259.
- 539 Manning, D.A.C., Rae, E.I.C., Gestsdóttir, K., 1994. Appraisal of the use of experimental and analogue  
540 studies in the assessment of the role of organic acid anions in diagenesis. Marine and Petroleum  
541 Geology 11(1), 10-19.
- 542 Masotta, M., Pontesilli, A., Mollo, S., Armienti, P., Ubide, T., Nazzari, M., Scarlato, P., 2020. The role of  
543 undercooling during clinopyroxene growth in trachybasaltic magmas: Insights on magma  
544 decompression and cooling at Mt. Etna volcano. Geochimica et Cosmochimica Acta 268, 258-276.
- 545 McHenry, L.J., 2009. Element mobility during zeolitic and argillic alteration of volcanic ash in a  
546 closed-basin lacustrine environment: Case study Olduvai Gorge, Tanzania. Chemistry Geology 265,  
547 540-552.
- 548 Meng, Y.L., Hu, Y., Li, X.N., Hu, A.W., Wu, C.L., Zhao, Z.T., Zhang, L., Xu, C., 2014. Controlling factors  
549 on physical property of tight volcanic rocks and reservoir quality prediction: a case study of the

- 550 Tiaohu formation in Malang-Tiaohu Sag. Oil and Gas Geology 35(2), 244-252.
- 551 Meshiri, I.D., 1986. On the reactivity of carbonic and organic acids and generation of secondary porosity.
- 552 The Society of Economic Paleontologists and Mineralogists 28, 123-128.
- 553 Minde, M.W., Wang, W.X., Madland, M.V., Zimmermann, U., Korsnes, R.I., Bertolino, S.R.A., Andersen,
- 554 P.Ø., 2018. Temperature effects on rock engineering properties and rock-fluid chemistry in
- 555 opal-CT-bearing chalk. Journal of Petroleum Science and Engineering 169, 454-470.
- 556 Nyland, R.E., Panter, K.S., Rocchi, S. Di Vincenzo, G., Del Carlo, P., Tiepolo, M., Field, B., Gorsevski, P.,
- 557 2013. Volcanic activity and its link to glaciation cycles: Single-grain age and geochemistry of Early to
- 558 Middle Miocene volcanic glass from ANDRILL AND-2A core, Antarctica. Journal of Volcanology
- 559 and Geothermal Research 250, 106-128.
- 560 Pang, H., Pang, X.Q., Dong, L., Zhao, X., 2018. Factors impacting on oil retention in lacustrine shale:
- 561 Permian Lucaogou Formation in Jimusaer Depression, Junggar Basin. Journal of Petroleum Science
- 562 and Engineering 163, 79-90.
- 563 Qiu, X.W., Liu, C.Y., Mao, G.Z., Deng, Y., Wang, F.F., Wang, J.Q., 2014. Late Triassic tuff intervals in the
- 564 Ordos basin, Central China: Their depositional, petrographic, geochemical characteristics and regional
- 565 implications. Journal of Asian Earth Sciences 80, 148-160.
- 566 Rowe, M.C., Ellis, B.S., Lindeberg, A., 2012. Quantifying crystallization and devitrification of rhyolites by
- 567 means of X-ray diffraction and electron microprobe analysis. American Mineralogist 97, 1685-1699.
- 568 Sell, B.K., Samson, S.D., Mitchell, C.E., McLaughlin, P.I., Koenig, A.E., Leslie, S.A., 2015. Stratigraphic
- 569 correlations using trace elements in apatite from Late Ordovician (Sandbian-Katian) K-bentonites of
- 570 eastern North America. GSA Bulletin 127, 1259-1274.
- 571 Surdam, R.C., Boese, S.W., Crossey, G.J., 1984. The chemistry of secondary porosity. AAPG Memoir 37,

- 572 127-151.
- 573 Surdam, R.C., Crossey, G.J., Hagen, E.S., 1989. Organic-inorganic and sandstone diagenesis. AAPG  
 574 Bulletin 73(1), 1-23.
- 575 Thomas Kalan, H.P., Sitorus, M.E., 1994. Jatibarang field, geologic study of volcanic reservoir for  
 576 horizontal well proposal. Indonesian Petroleum Association, 23<sup>rd</sup> Annual Convention Proceedings 1,  
 577 229-244.
- 578 Tian, Y., Xiong, Y., Wang, L., Lei, Z.D., Zhang, Y., Yin, X.L., Wu, Y.S., 2019. A compositional model for  
 579 gas injection IOR/EOR in tight oil reservoirs under coupled nanopore confinement and geomechanics  
 580 effects. Journal of Natural Gas Science and Engineering 71, 102973.
- 581 Tomaru, H., Lu, Z.L., Fehn, U., Muramatsu, Y., 2009. Origin of hydrocarbons in the Green Tuff region of  
 582 Japan: 129I results from oil field brines and hot springs in the Akita and Niigata Basins. Chemical  
 583 Geology 264, 221-231.
- 584 Tsukamoto, S., Rink, W.J., Watanuki, T., 2003. OSL of tephric loess and volcanic quartz in Japan and an  
 585 alternative procedure for estimating De from a fast OSL component. Radiation Measurements 37(4-5),  
 586 459-465.
- 587 Wang, J., Cao, Y.C., Liu, K.Y., Gao, Y., Qin, Z.J., 2019. Fractal characteristics of the pore structures of  
 588 fine-grained, mixed sedimentary rocks from the Jimsar Sag, Junggar Basin: Implications for lacustrine  
 589 tight oil accumulations. Journal of Petroleum Science and Engineering 182, 106363.
- 590 Wang, P.J., Chen, S.M., 2015. Cretaceous volcanic reservoirs and their exploration in the Songliao Basin,  
 591 northeast China. AAPG Bulletin 99(3), 499-523.
- 592 Wang, S.J., Yu, Y.J., Guo, Q.L., 2014. New advance in resources evaluation of tight oil. Acta Petrolei  
 593 Sinica 35(6), 1095-1105.

- 594 Wark, D.A., Hildreth, W., Spear, F.S., Cherniak, D.J., Watson, E.B., 2007. Pre-eruption recharge of the  
 595 Bishop Magma system. *Geology* 35, 235-238.
- 596 Wei, W., Zhu, X.M., He, M.W., Wang, M.W., Liu, X.B., 2018. Original sediment composition of the Lower  
 597 Cretaceous lacustrine tight-oil mudstone and influences on diagenesis and organic matter content, the  
 598 Erennaer Sag in Erlian Basin, NE China. *Marine and Petroleum Geology* 94, 131-143.
- 599 Winchester, J.A., Floyd, P.A., 1977. Geochemical discrimination of different magma series and their  
 600 differentiation products using immobile elements. *Chemistry Geology* 20, 325-343.
- 601 Wolff, D., Gislason, S.R., Oelkers, E.H., Putnis, C.V., 2004. The dissolution rates of natural glasses as a  
 602 function of their composition at pH 4 and 10.6, and temperatures from 25 to 74 °C. *Geochimica et  
 603 Cosmochimica Acta* 68, 4843-4858.
- 604 Xu, H., Tang, D.Z., Zhang, J.F., 2013. Coexistence mechanism of multi-types of reservoir pressure in the  
 605 Malang depression of the Santanghu basin, China. *Journal of Petroleum Science and Engineering* 108,  
 606 279-287.
- 607 Xu, H., Zhou, W., Zhang, R., Liu, S.M., Zhou, Q.M., 2018 Characterizations of pore, mineral and  
 608 petrographic properties of marine shale using multiple techniques and their implications on gas  
 609 storage capability for Sichuan Longmaxi gas shale field in China. *Fuel* 241, 360-371.
- 610 Yang, S.C., Hu, W.X., Wang, X.L., Jiang, B.Y., Yao, S.P., Sun, F.N., Huang, Z.C., Zhu, F., 2019. Duration,  
 611 evolution, and implications of volcanic activity across the Ordovician–Silurian transition in the Lower  
 612 Yangtze region, South China. *Earth and Planetary Science Letters* 518, 13-25.
- 613 Yang, R., Hao, F., He, S., He, C.C., Guo, X.S., Yi, J.Z., Hu, H.Y., Zhang, S.W., Hu, Q.H., 2017.  
 614 Experimental investigations on the geometry and connectivity of pore space in organic-rich Wufeng  
 615 and Longmaxi shales. *Marine and Petroleum Geology*, 84(6), 225-242.

- 616 Yuan, W., Liu, G.D., Stebbins, A., Xu, L.M., Niu, X.B., Luo, W.B., Li, C.Z., 2017. Reconstruction of redox  
 617 conditions during deposition of organic-rich shales of the Upper Triassic Yanchang Formation, Ordos  
 618 Basin, China. *Palaeogeography, Palaeoclimatology, Palaeoecology* 486, 158-170.
- 619 Zhang, B.Q., Yu, H.Z., Jiang, Z.X., Wang, Y.J., Wang, W.H., 2003. Characteristics and diagenetic  
 620 environments of source rocks by cathodoluminescence. *Petroleum Exploration and Development* 30,  
 621 117-120.
- 622 Zhang, J.Y., Liu, G.D., Cao, Z., Tao, S.Z., Felix, M., Kong, Y.H., Zhang, Y.Y., 2019. Characteristics and  
 623 formation mechanism of multi-source mixed sedimentary rocks in a saline lake, a case study of the  
 624 Permian Lucaogou Formation in the Jimusaer Sag, northwest China. *Marine and Petroleum Geology*  
 625 102, 704-724.
- 626 Zhao, X.Z., Li, Q., Jiang, Z.X., Zhang, R.F., Li, H.P., 2013. Organic geochemistry and reservoir  
 627 characterization of the organic matter-rich calcilutite in the Shulu Sag, Bohai Bay Basin, North China.  
 628 *Marine and Petroleum Geology* 51, 239-255.
- 629 Zhao, X.Z., Zhou, L.H., Pu, X.G., Jin, F.M., Han, W.Z., Xiao, D.Q., Chen, S.Y., Shi, Z.N., Zhang, W., Yang,  
 630 F., 2018. Geological characteristics of shale rock system and shale oil exploration breakthrough in a  
 631 lacustrine basin: A case study from the Paleogene 1st sub-member of Kong 2 Member in Cangdong  
 632 sag, Bohai Bay Basin, China. *Petroleum Exploration and Development* 45(3), 377-388.
- 633 Zhao, Z.H., Guo, Z.J., Zhang, C., 2003. Tectonic evolution of the Santanghu Basin, east Xinjiang and its  
 634 implication for the hydrocarbon accumulation. *Acta Scientiarum Naturalium Universitatis Pekinensis*  
 635 39(2), 219-228. (in Chinese with English abstract)
- 636 Zhu, S.F., Zhu, X.M., Liu, J.S., Yao, Y., Xian, B.Z., Niu, H.P., Zhao, C.Y., 2012. Genesis and hydrocarbon  
 637 significance of vesicular ignimbrite: A case study from Fengcheng Formation, Wu-Xia area, Junggar

- 638 Basin, NW China. Petroleum Exploration and Development 39(2), 162-171.
- 639 Zhu, S.F., Zhu, X.M., Liu, X.C., Li, C., Wang, X.X., Tan, M.X., Geng, M.Y., Li, Y.P., 2014. Alteration
- 640 products of volcanic materials and their influence on reservoir space in hydrocarbon reservoirs:
- 641 evidence from Lower Permian strata in Ke-Xia region, Junggar Basin. Acta Petrolei Sinica 35(2),
- 642 276-285.
- 643 Zhu, Y.F., Zhang, L.F., Gu, L.B., Guo, X., 2005. The zircon shrimp chronology and trace element
- 644 geochemistry of the Carboniferous volcanic rocks in western Tianshan Mountains. Chinese Science
- 645 Bulletin 50, 2201-2212.
- 646

## Tables

**Table 1** The relative content of different minerals of the Tiaohu and Haerjiawu Formation tuffs from XRD analysis

Wells	Depth (m)	Formation	The relative content of minerals (%)					
			Quartz	Potassium feldspar	Albite	Anorthite	Clay minerals	Calcite
L1*	2547.47	Tiaohu	45	6	11	-	5	33
L1*	2547.86	Tiaohu	75	-	16	-	7	2
L1*	2548.78	Tiaohu	76	6	8	-	4	6
L1*	2548.7-2548.8	Tiaohu	56	-	20	-	9	15
L1*	2548.9	Tiaohu	47	-	15	-	11	27
M56*	2141.6-2141.8	Tiaohu	63	-	33	-	-	4
M56*	2142.2-2142.3	Tiaohu	57	-	36	-	-	7
M56*	2142.5-2142.6	Tiaohu	51	-	35	-	4	10
M56*	2142.8-2142.96	Tiaohu	67	-	29	-	4	-
M56*	2143.6-2143.7	Tiaohu	43	-	42	-	9	6
M56*	2144.1-2144.4	Tiaohu	49	-	46	-	5	-
M56*	2144.9-2144.6	Tiaohu	32	-	58	-	-	10
M56*	2144.73	Tiaohu	69	-	19	-	4	8
M56*	2145.3-2145.4	Tiaohu	36	-	57	-	4	3
M7*	1790.8-1790.9	Tiaohu	66	-	9	-	14	11
M7*	1885.06	Tiaohu	57	-	37	-	6	-
M56-12H*	2112.7-2112.8	Tiaohu	78	-	15	-	7	-
M56-12H*	2118.2-2118.3	Tiaohu	52	-	36	-	12	-
M56-12H*	2118.4-2118.5	Tiaohu	58	-	23	-	19	-
M56-12H*	2118.9-2119.1	Tiaohu	68	-	28	-	4	-
M56-12H*	2122.4-2122.6	Tiaohu	45	-	38	-	17	-
M56-12H*	2125.7-2125.9	Tiaohu	57	-	36	-	7	-
M36	2311.1	Haerjiawu	9	-	-	50	19	22
M361	3167.4-3167.6	Haerjiawu	11	-	-	15	10	-
M38	3037.89	Haerjiawu	10	-	-	33	6	45
M40	2583.9-2584.1	Haerjiawu	25	-	-	39	8	4
M40	2733.4-2733.5	Haerjiawu	35	-	46	-	12	3
M40	2734.2-2734.5	Haerjiawu	21	-	34	-	24	2
								19

“\*” means data collected from Jiao et al., 2014; Ma et al., 2016.

**Table 2** Porosity data of different tuffs in the Tiaohu Formation

Wells	Depth (m)	Formation	Lithology	Porosity (%)	Permeability (mD)
M21	1775.1	Haerjiawu	lithic tuff	11.98	0.025
M27	2733.4	Haerjiawu	lithic tuff	12.64	0.054
M36	2311.1	Haerjiawu	lithic tuff	4.4	0.017
M38	3037.89	Haerjiawu	lithic tuff	0.9	0.00076
M40	2733.4	Haerjiawu	lithic tuff	12.6	0.02
M45	2485.1	Haerjiawu	lithic tuff	5.1	0.058
M67H	2536.29	Haerjiawu	lithic tuff	6.4	0.079
M40	2733.85	Haerjiawu	lithic tuff	10.4	0.08
M33	1870.23	Haerjiawu	lithic tuff	5.9	0.083
M33	2720.77	Haerjiawu	lithic tuff	5.1	0.092
M361	3155.5	Haerjiawu	lithic tuff	1.6	0.25
M361	3163.3	Haerjiawu	lithic tuff	2.3	0.3
M361	3167.36	Haerjiawu	lithic tuff	3.8	0.00017
M361	3170.4	Haerjiawu	lithic tuff	6.3	0.048
M361	3171.1	Haerjiawu	lithic tuff	2.5	0.095
M361	3175.3	Haerjiawu	lithic tuff	1.7	0.045
M55	2266.8	Tiaohu	crystal tuff	9.1	0.046
M55	2268.00	Tiaohu	crystal tuff	7.1	0.089
M55	2269.15	Tiaohu	crystal tuff	10.5	0.08
M55	2270.11	Tiaohu	crystal tuff	8.7	0.0344
M55	2270.33	Tiaohu	crystal tuff	10.8	0.0058
M55	2270.5	Tiaohu	crystal tuff	8.41	0.046
L1	2547.86	Tiaohu	vitric tuff	21.0	0.15
L1	2548.57	Tiaohu	vitric tuff	24.0	0.052
L1	2548.78	Tiaohu	vitric tuff	24.3	0.0617
M55	2476.25	Tiaohu	vitric tuff	23.1	0.0026
M55	2476.42	Tiaohu	vitric tuff	19.4	0.067
M55	2476.55	Tiaohu	vitric tuff	20.6	0.03
M56	2141.60	Tiaohu	vitric tuff	18.5	0.049
M56	2142.50	Tiaohu	vitric tuff	22.7	0.087
M56	2142.96	Tiaohu	vitric tuff	21.6	0.063
M56	2144.10	Tiaohu	vitric tuff	13.3	0.00056
M56	2145.30	Tiaohu	vitric tuff	17.3	0.059
M56	2144.99	Tiaohu	vitric tuff	21.0	0.2022
M56-12H*	2116.66	Tiaohu	vitric tuff	15.4	--
M56-12H*	2126.90	Tiaohu	vitric tuff	22.6	--
M56-12H*	2127.67	Tiaohu	vitric tuff	13.3	--
M56-12H*	2128.38	Tiaohu	vitric tuff	18.6	--
M7*	1790.8	Tiaohu	vitric tuff	18.8	--
M1	--	Tiaohu	vitric tuff	16.4	0.016
M15	--	Tiaohu	vitric tuff	17.77	0.011

M56	--	Tiaohu	vitric tuff	18.9	0.086
L1	2547.7	Tiaohu	vitric tuff	29.13	0.13
L1*	2548.46~2548.53	Tiaohu	vitric tuff	23.6	--
L1*	2548.99~2549.11	Tiaohu	vitric tuff	16.3	--
M56	2142.96~2143.08	Tiaohu	vitric tuff	21.6	0.012
M56	2145.68~2145.75	Tiaohu	vitric tuff	21.9	0.012

“\*” means data collected from Jiao et al., 2014; Ma et al., 2016.

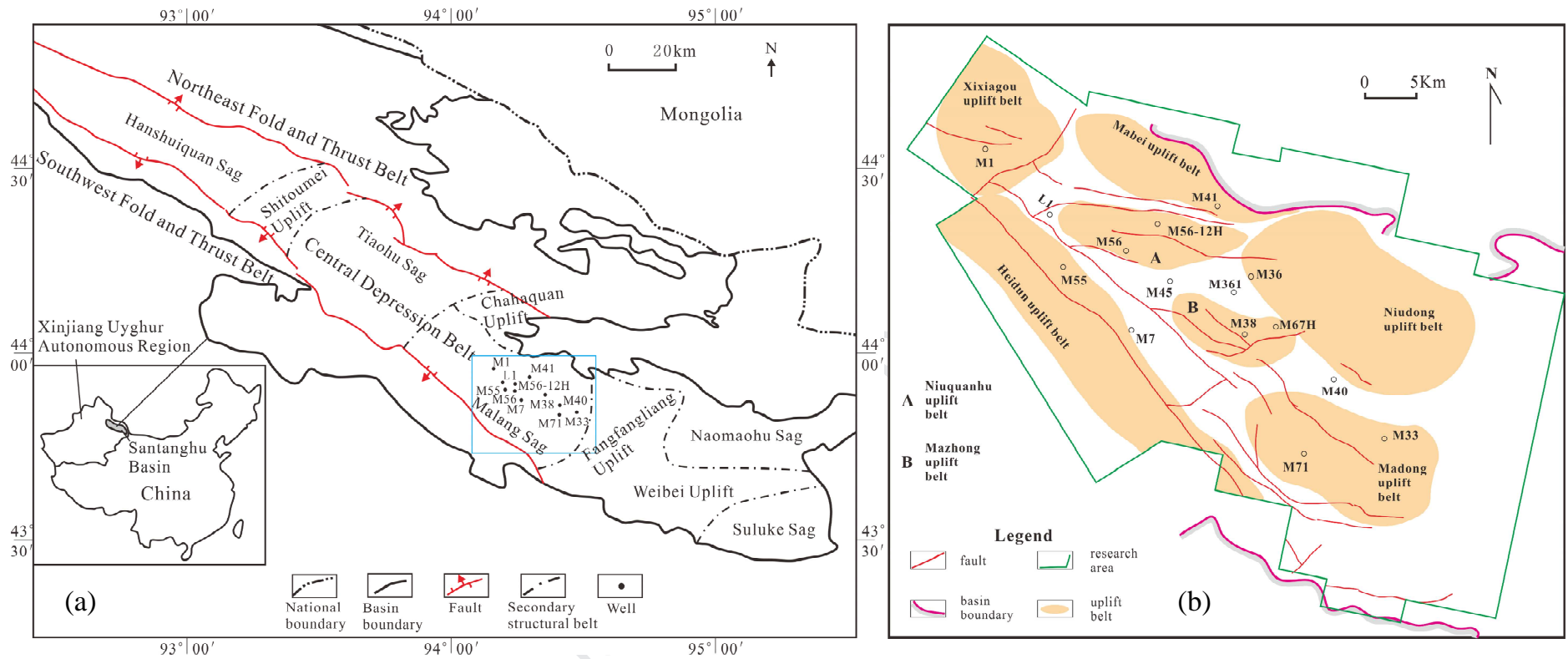


**Fig. 1.** Location map of the Santanghu Basin (a) and wells in Malang Sag (b), NW China.

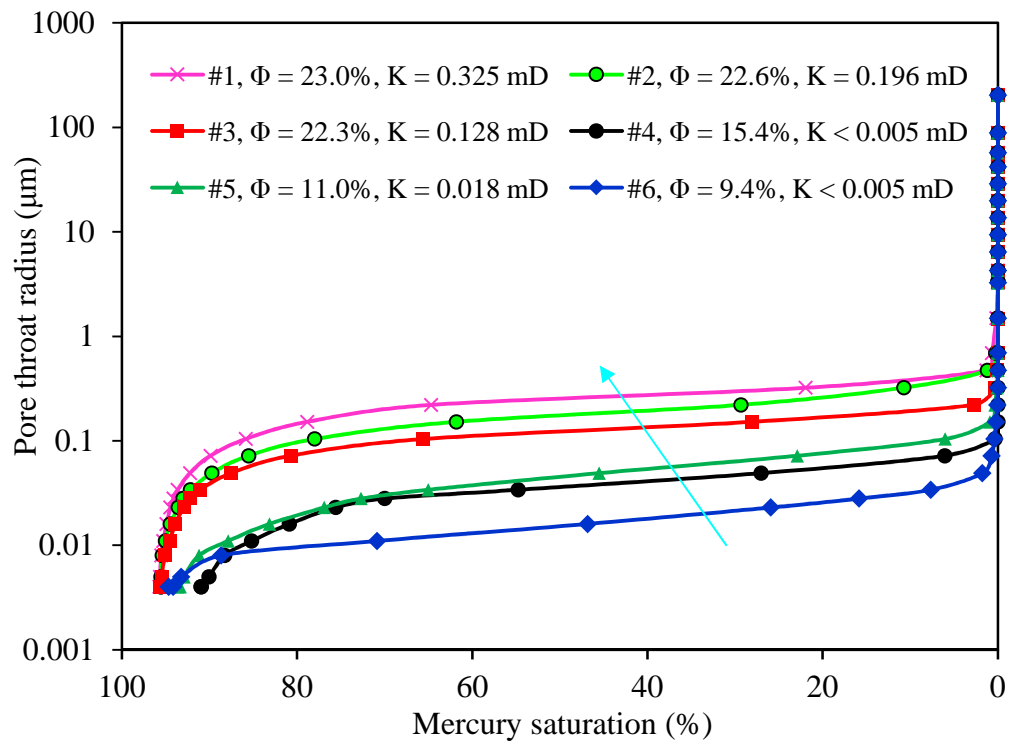


**Fig. 10.** Pore throat radius distribution characteristics of typical tuff samples in the Tiaohu Formation, which shows that the pore throat radii of the tuff are generally  $<1.0 \mu\text{m}$  (mostly  $<0.1 \mu\text{m}$ ) (Ma et al., 2016).  $\Phi$  = Porosity;  $K$  = Permeability.

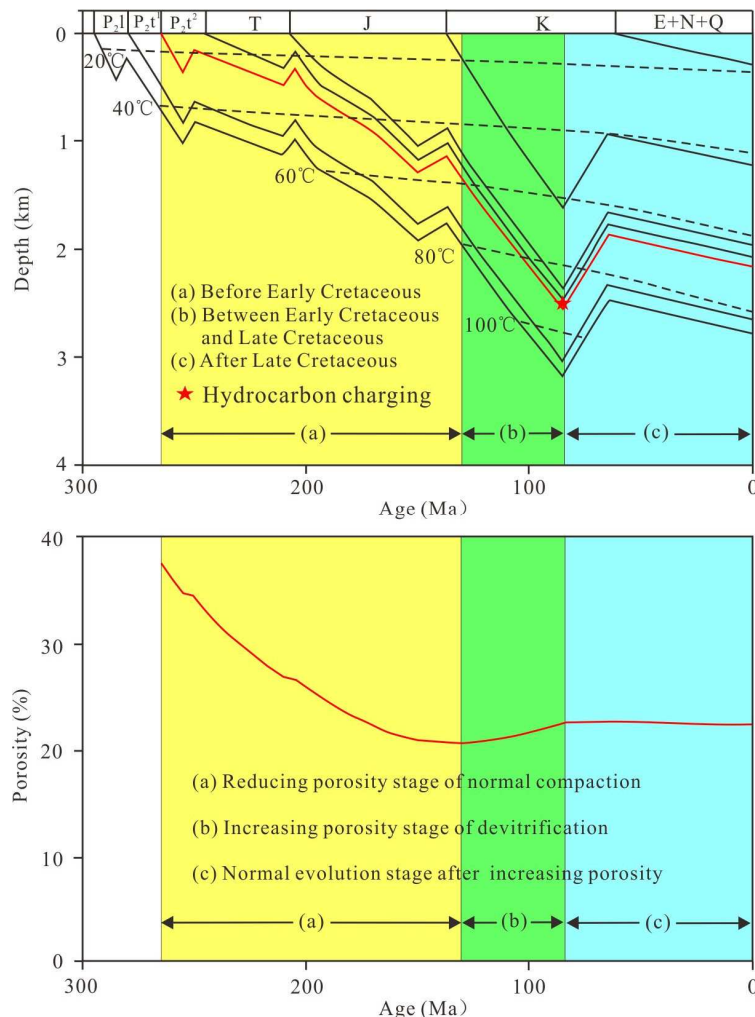


**Fig. 11.** Burial history of Well M56 and porosity evolution characteristics of the tuff in the Tiaohu Formation in the Malang Sag.

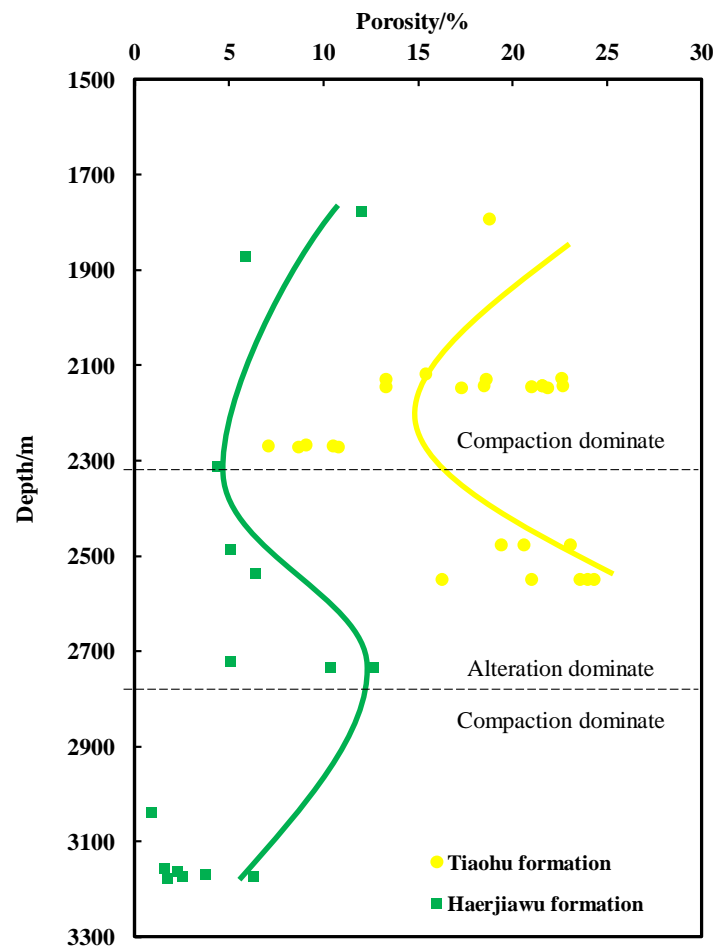
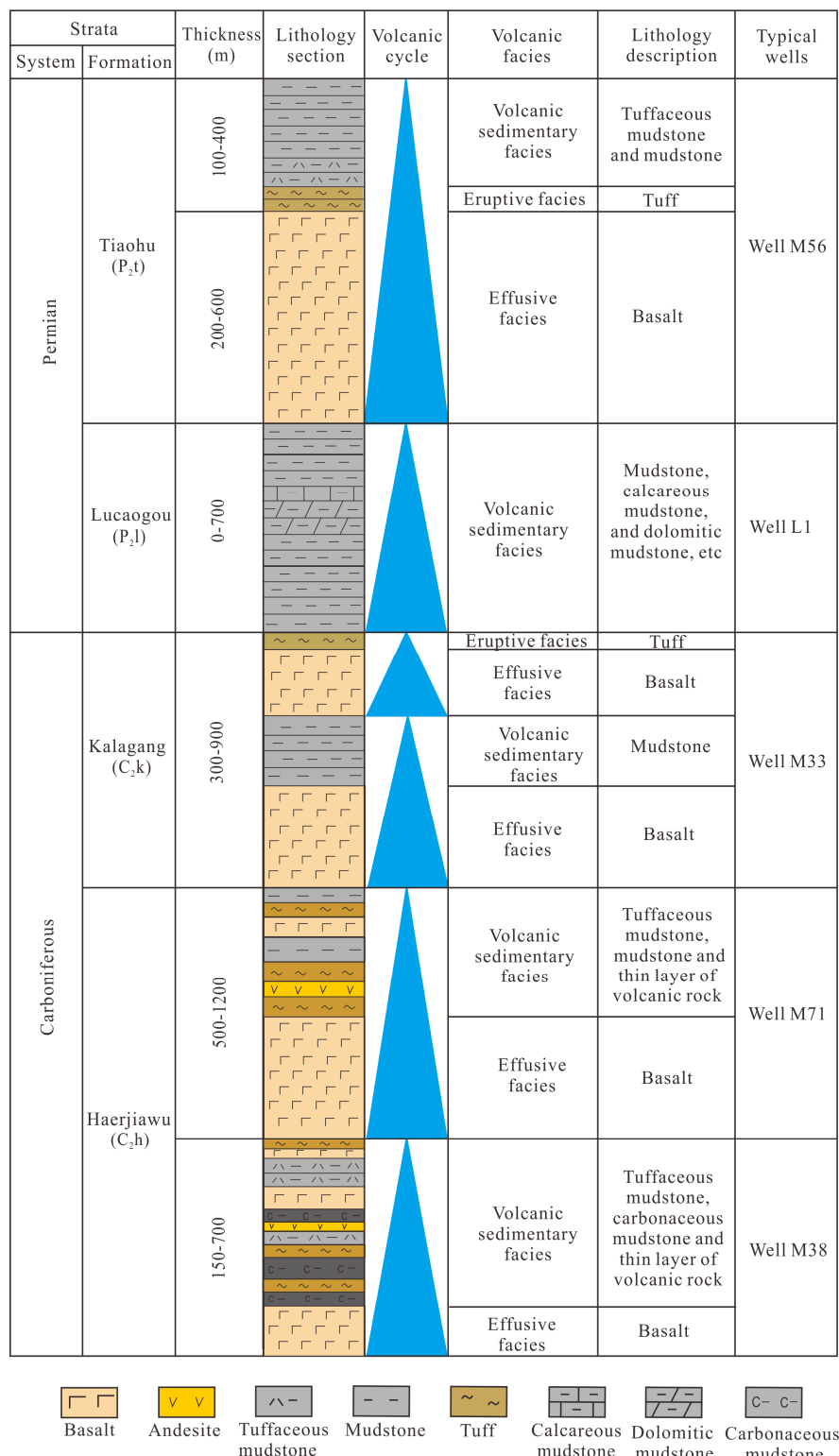
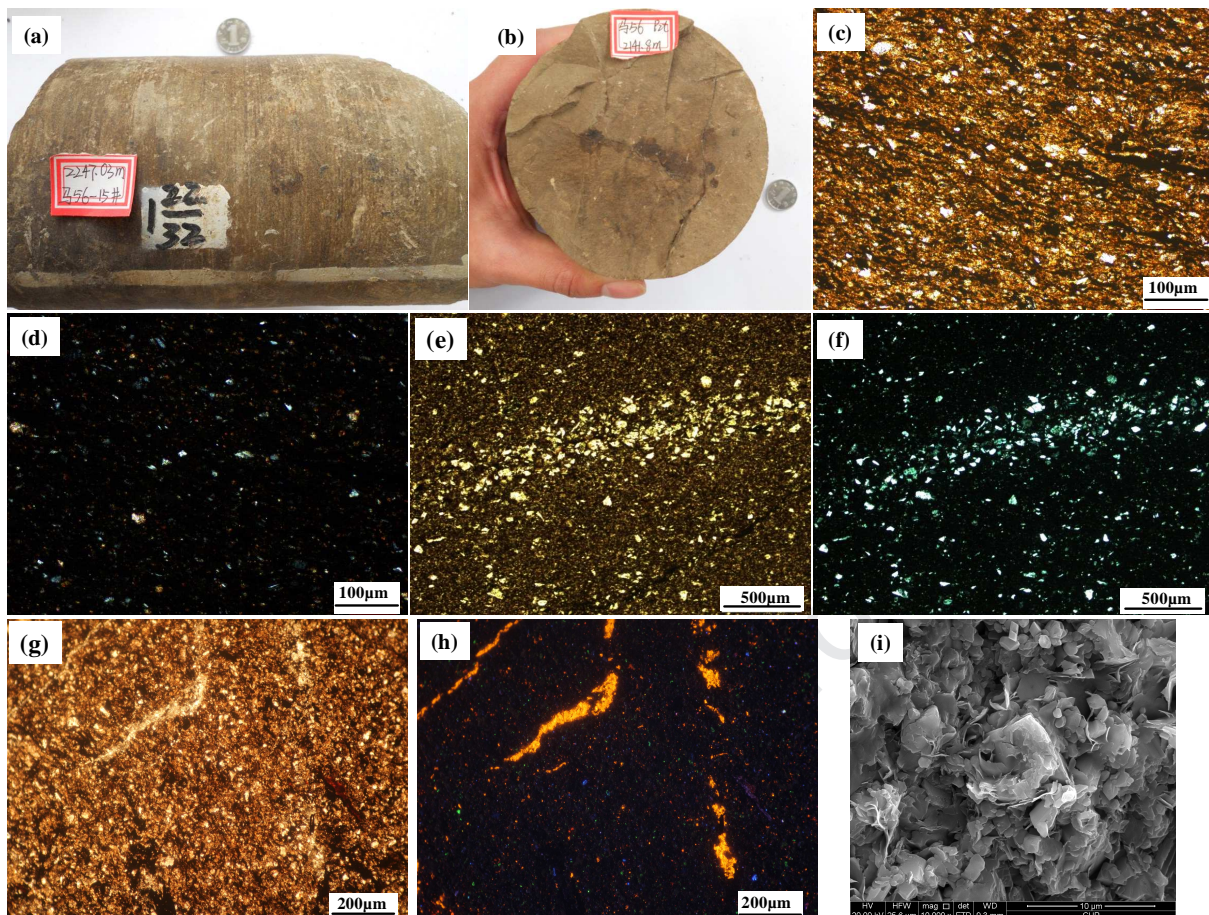


Fig. 12 Plot of depth versus porosity for the Tiaohu and Haerjiawu formations samples



**Fig. 2.** Comprehensive columnar section of volcanic cycles in the Santanghu Basin, which shows two relatively complete volcanic cycles in the Carboniferous Haerjiawu Formation and Kalagang Formation, one volcanic cycle in the Permian Lucaogou Formation and Tiaohu Formation, respectively.



**Fig. 3.** Petrographic characteristics of tuffs in the Tiaohu Formation. (a) Massive and earthy yellow tuff. Matrix contains oil. Core of Well M56-15, 2247.03 m. (b) Massive and earthy yellow tuff. Both matrix and fractures contain oil. Core of Well M56, 2141.8 m. (c) Vitric tuff. Core of Well M56, 2142.96 m, thin section (polarized light). (d) Same source as (c). Obvious extinction is observed under cross-polarized light. (e) Crystal tuff. Core of Well M56-15H, 2252.34 m, thin section (polarized light). (f) Same source as (e). Crystal fragments do not show extinction and other parts have obvious extinction under cross-polarized light. (g) Vitric tuff. Core of Well M56, 2142.18 m, thin section (polarized light). (h) Same source as (g). (i) Vitric tuff. Core of Well M56, 2143 m. Arrows point to non-luminescent quartz, showing authigenic quartz formed by alteration. Thin section (cathodoluminescence).

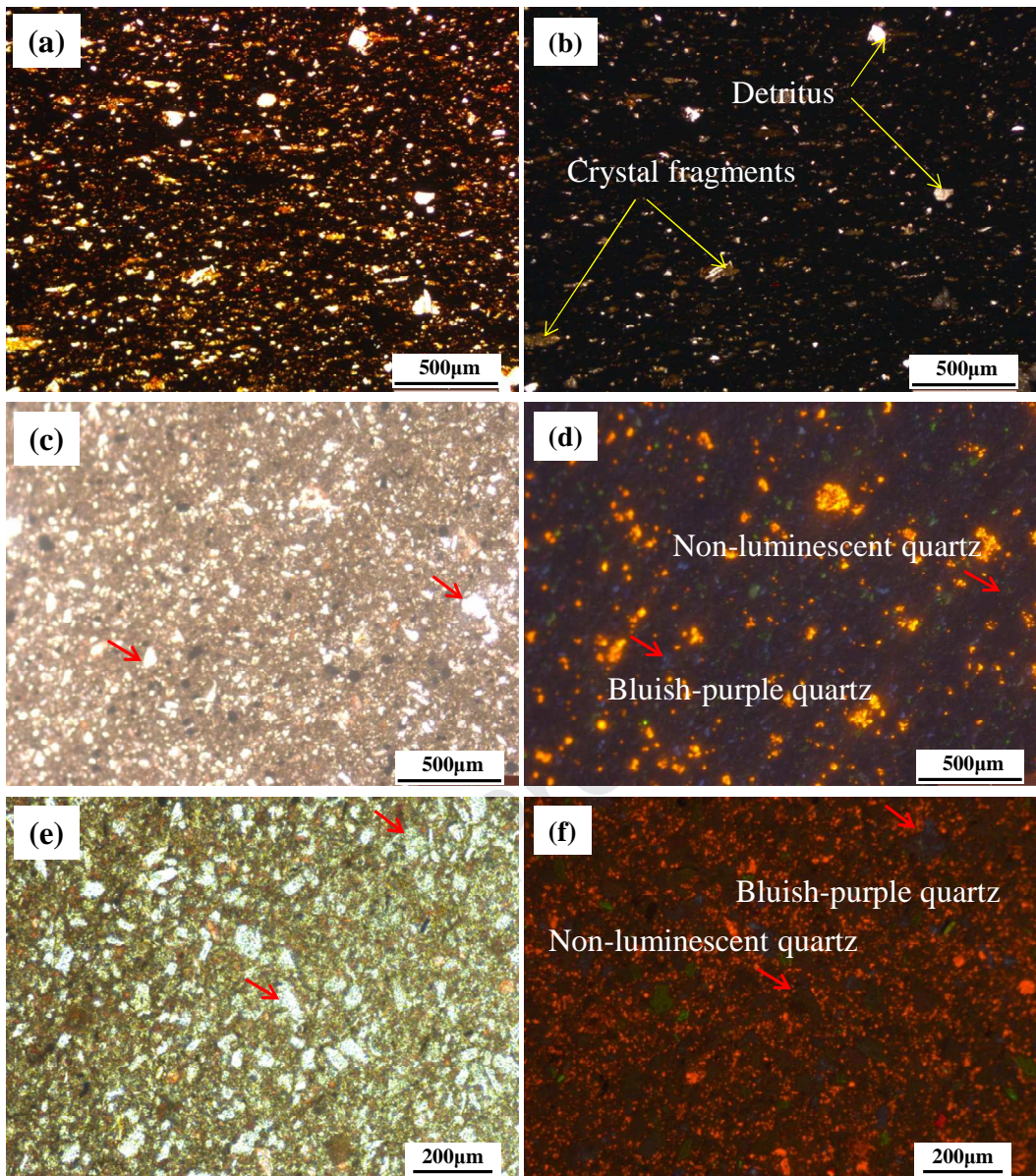


**Fig. 4.** Petrographic characteristics of tuffs in the Haerjiawu Formation. (a) Tuff consists of crystal fragments and detritus. Core of Well M33, 2721.62 m. Thin section (polarized light). (b) Same source as (a). Thin section (cross-polarized light). (c) Core of Well M40, 2734.2 m. Thin section (polarized light). (d) Same source as (c), Thin section (cathodoluminescence). (e) Core of Well M56, 2143 m. Thin section (polarized light). (f) Same source as (e), Thin section (cathodoluminescence). Arrows point to non-luminescent quartz and bluish-purple quartz, showing authigenic quartz formed by alteration and high-temperature quartz formed by volcanism, respectively.

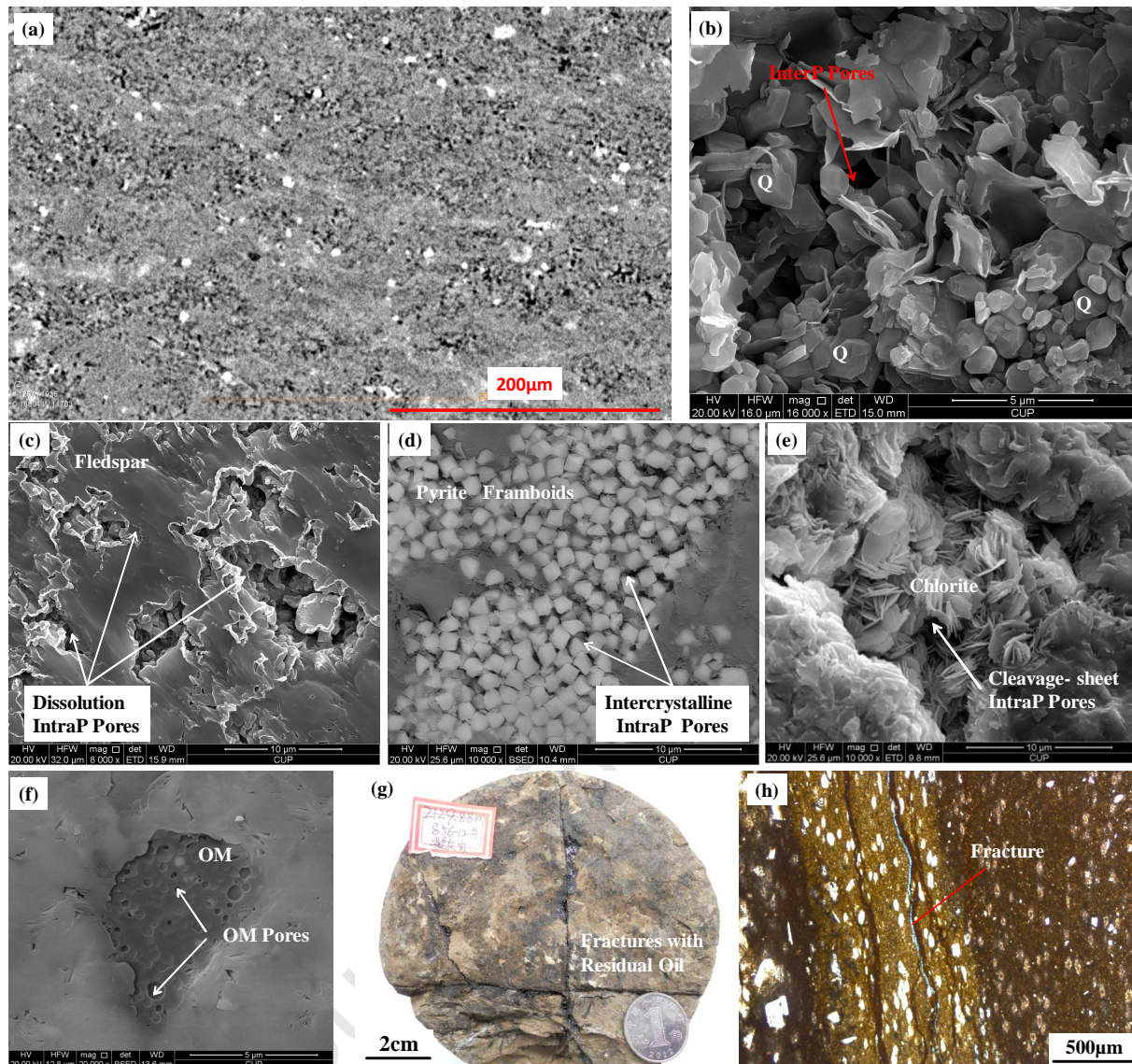


**Fig. 5.** Example of different micropores in the tuffs of the Tiaohu Formation (Ma et al., 2016). (a) Micropores observed by CT scanning, Well M56-12H, 2118.4 m. (b) Interparticle (InterP) pores between quartz caused by alteration. Well M56, 2143.3 m. Observed by SEM. (c) Dissolution intraparticle (IntraP) pores within a large feldspar grain. Well M56, 2143.3m. Observed by SEM. (d) Intercrystalline intraparticle (IntraP) pores within pyrite frambooids. Well L1, 2548.7 m. BSED image. (e) Cleavage-sheet intraparticle (IntraP) pores within chlorite. Core of Well M56, 2142.5 m. Observed by SEM. (f) Micropores within organic matter (OM). Well L1, 2548.7 m. BSED image. (g) Fractures with residual oil. Core sample of Well M56-12H, 2129.88 m. (h) Opening-mode microfracture. Well M56, 2142.9 m. Abbreviations: det = detector; WD = working distance; mag = magnification; HV = high voltage; HFW = horizontal frame width; spot = spot size; BSED = backscattered electron detector.

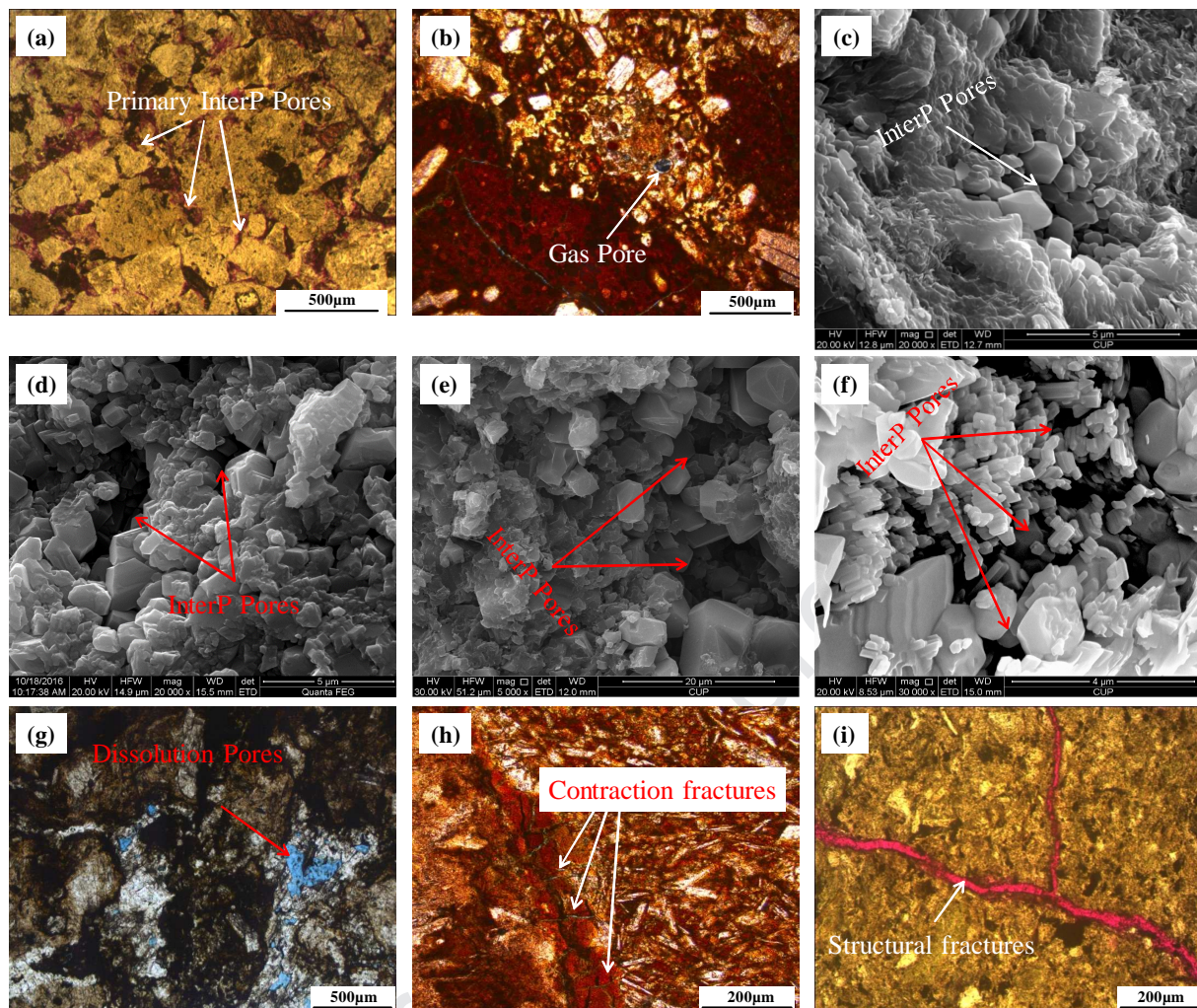


**Fig. 6.** Example of different micropores in the tuffs of the Haerjiawu Formation. (a) Primary interparticle pores. Well M704, 3469.3 m. (b) Primary gas pores. Well M361, 3163.02 m. (c) Interparticle (InterP) pores between minerals caused by alteration. Well M38, 3037.2 m. Observed by SEM. (d~f) Interparticle (InterP) pores between minerals caused by alteration. Well M56, 2143.33 m. Observed by SEM. (g) Dissolution pores. Well M40, 2364.46 m. (h) Contraction fractures. Well ND201, 3153.75 m. (i) Structural fractures. Well M704, 3437.9 m.

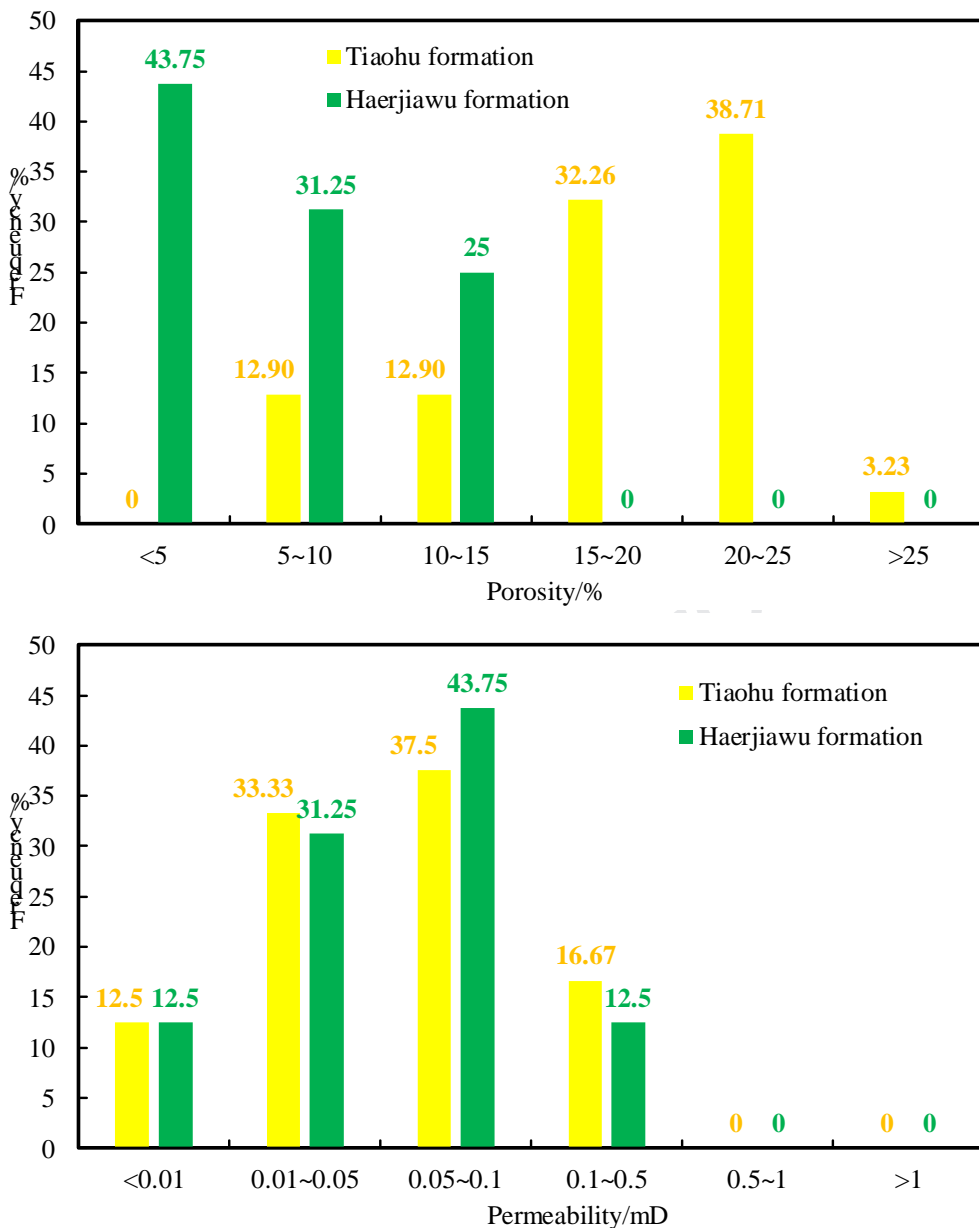


**Fig. 7.** Distributions of porosity and permeability of the tuffs. It shows that the tuffs of the Tiaohu Formation are characterized by moderate-high porosity and low permeability, and the tuffs of the Haerjiawu Formation are characterized by low porosity and low permeability.

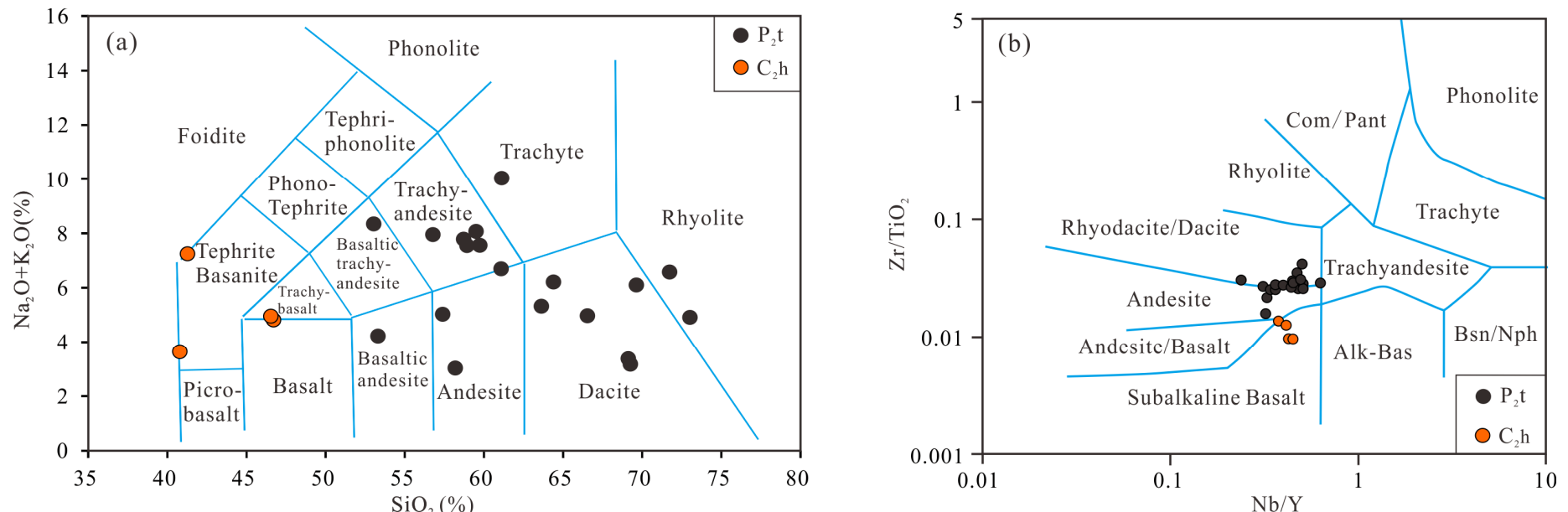


**Fig. 8.** (a) Classification of tuffs in TAS (after Le Bas et al., 1986). (b)  $\text{Nb}/\text{Y}$ - $\text{Zr}/\text{TiO}_2$  discrimination diagram for the tuffs (after Winchester and Floyd, 1977). The data of the Tiaohu formation are from Ma et al., 2016.

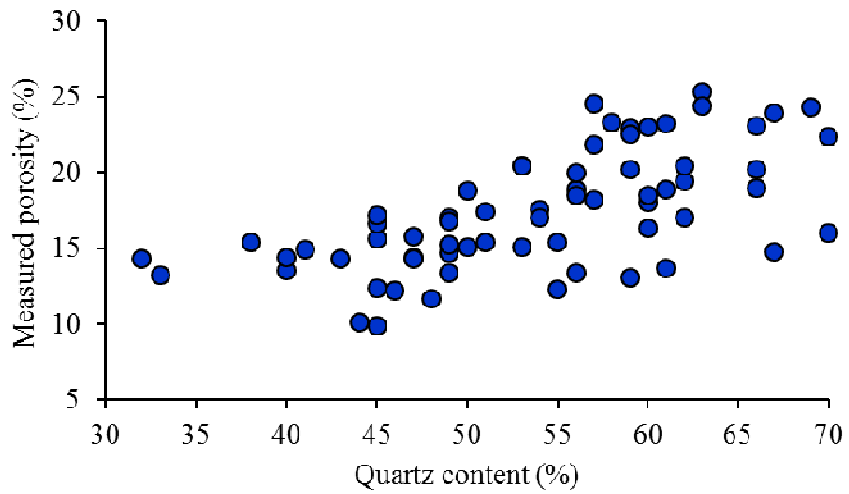


**Fig. 9.** Plot of quartz content versus porosity of the Tiaohu Formation tuffs, which shows a positive relationship between them.

Highlights:

- (1) The Tiaohu Formation tuff reservoir is characterized by higher porosity than that of the Haerjiawu Formation
- (2) Alteration and compaction processes contributed most to the pore formation in the two sets of tuff reservoir
- (3) The nature of tuff and deeper burial depth are the major reasons for a worse physical properties of Haerjiawu Formation tuff reservoir

**1    Author Contributions**

- 2    The manuscript was written through contributions of all authors. All authors have given approval to the  
3    final version of the manuscript.

**1 Notes**

2 The authors declare no competing financial interest.